(2)

ASPECTS OF RAMAN SCATTERING

Final Report

JAYCOR Report Number J206-89-002/6264

August 25, 1989

JAYCOR

1608 Spring Hill Road
Vienna, Virginia 22180-2270

JAYCOR

(2)

ASPECTS OF RAMAN SCATTERING

Final Report

JAYCOR Report Number J206-89-002/6264

August 25, 1989

Final Report by:

Rita Mahon
David G. Cooper
James L. Dexter

Prepared for:

Naval Research Laboratory
4555 Overlook Avenue, SW
Washington, DC 20375-5000

Under:
Contract Number N00014-87-C-2013

1608 Springhill Road • Vienna, Virginia 22180-2270 • (703) 847-4000

JAYCOR

August 25, 1989

Dr. Bernard Wexler
Code 6544
Naval Research Laboratory
4555 Overlook Avenue, SW
Washington, DC 20375-5000

SUBJECT: Final Report, Contract Number N00014-87-C-2013

Dear Dr. Wexler:

JAYCOR is pleased to submit this Final Report entitled, "Aspects of Raman Scattering," in accordance with the subject contract, CDRL Item Number A003.

If the Final Report is acceptable, please sign and forward the enclosed DD Form 250.

Questions of a technical nature should be addressed to Dr. Rita Mahon while questions of a contractual nature should be addressed to Ms. Barbara Ballard, our Contracts Administrator.

Sincerely,

Martin C. Nielsen
Vice President and
General Counsel

ssh

Enclosure

cc: Code 6542 (3 copies)
Code 2627 (6 copies)
DTIC (12 copies)

1608 Springhill Road • Vienna, Virginia 22180-2270 • (703) 847-4000

UNCLASSIFIED
SECURITY CLASSIFICATION OF THIS PAGE

REPORT DOCUMENTATION PAGE

1a. REPORT SECURITY CLASSIFICATION UNCLASSIFIED	1b. RESTRICTIVE MARKINGS N/A
2a. SECURITY CLASSIFICATION AUTHORITY N/A	3. DISTRIBUTION/AVAILABILITY OF REPORT A/Unlimited Distribution
2b. DECLASSIFICATION/DOWNGRADING SCHEDULE N/A	
4. PERFORMING ORGANIZATION REPORT NUMBER(S) J206-89-002/6264	5. MONITORING ORGANIZATION REPORT NUMBER(S)
6a. NAME OF PERFORMING ORGANIZATION JAYCOR — 6b. OFFICE SYMBOL (If applicable)	7a. NAME OF MONITORING ORGANIZATION Naval Research Laboratory
6c. ADDRESS (City, State, and ZIP Code) 1608 Spring Hill Road Vienna, VA 22182	7b. ADDRESS (City, State, and ZIP Code) 4555 Overlook Avenue, SW Washington, DC 20375
8a. NAME OF FUNDING/SPONSORING ORGANIZATION Naval Research Laboratory — 8b. OFFICE SYMBOL (If applicable) Code 6544	9. PROCUREMENT INSTRUMENT IDENTIFICATION NUMBER N00014-87-C-2013
8c. ADDRESS (City, State, and ZIP Code) 4555 Overlook Avenue, SW Washington, DC 20375	10. SOURCE OF FUNDING NUMBERS PROGRAM ELEMENT NO.: A003 — PROJECT NO. — TASK NO. — WORK UNIT ACCESSION NO.
11. TITLE (Include Security Classification) *Aspects of Raman Scattering (U)*	
12. PERSONAL AUTHOR(S) Rita Mahon, David G. Cooper & James L. Dexter	
13a. TYPE OF REPORT Final Report — 13b. TIME COVERED FROM 12/01/86 TO 04/30/89 — 14. DATE OF REPORT (Year, Month, Day) 89 AUG 25 — 15. PAGE COUNT 70 pages	
16. SUPPLEMENTARY NOTATION	

17. COSATI CODES			18. SUBJECT TERMS (Continue on reverse if necessary and identify by block number)
FIELD	GROUP	SUB-GROUP	Stimulated Raman scattering; Stokes generation; atmospheric propagation; unstable resonator cavity; beam clean-up; Raman gain suppression.

19. ABSTRACT (Continue on reverse if necessary and identify by block number)

We have investigated a number of aspects of stimulated Raman scattering with a view to a better understanding of the propagation of intense light beams through the atmosphere. In addition, we have developed new unstable resonator cavities for the long pulse excimer laser used in the Raman beam-cleanup experiments and have made preliminary measurements on an anti-Stokes Raman laser which operates in the vacuum ultra violet region of the spectrum. In particular, we have conducted experiments which demonstrate the Raman gain suppression observed on-axis, or at very small angles, for rotational Raman gain using linearly polarized beams in hydrogen and deuterium. We have also demonstrated and measured the reduction in vibrational Raman gain at the phase matching angle in hydrogen and deuterium. The normal exponential gain observed in the transient limit has been modeled to fit our experiment. The theory had to take account of the actual beam shapes, both spatially and temporally, as well as the self-phase modulation, in order to correctly predict the observed gain functions. We have also performed experiments on the beam quality and gain dependence of the

20. DISTRIBUTION/AVAILABILITY OF ABSTRACT ☐ UNCLASSIFIED/UNLIMITED ☒ SAME AS RPT. ☐ DTIC USERS	21. ABSTRACT SECURITY CLASSIFICATION UNCLASSIFIED
22a. NAME OF RESPONSIBLE INDIVIDUAL Dr. Bernard Wexler	22b. TELEPHONE (Include Area Code) (202)767-2813 — 22c. OFFICE SYMBOL Code 6544

DD FORM 1473, 84 MAR — 83 APR edition may be used until exhausted. All other editions are obsolete.

SECURITY CLASSIFICATION OF THIS PAGE
UNCLASSIFIED

19. ABSTRACT (Continued)
2nd Stokes. In particular, a study of the seeding mechanism responsible for generating the 2nd Stokes through the threshold level, has required statistical, spectral, beam profile and gain parameter studies. We also report on crossed pump beam experiments where the beam quality was determined by simultaneous measurements of the beam profile in both the near and the far field. The far field pattern was then compared with the Fourier transform of the near field pattern to give a measure of the beam quality. Pulse energy statistics of the self-generated Stokes as well as of amplified and saturated Stokes have been studied from the point of view of Raman beam control. Such studies have mainly been restricted to Fresnel number 1 systems although larger Fresnel number 10 systems have been studied by the control exerted over the spatial patterns.

Accession For	
NTIS GRA&I	☑
DTIC TAB	☐
Unannounced	☐
Justification	
By	
Distribution/	
Availability Codes	
Dist	Avail and/or Special
A-1	

TABLE OF CONTENTS

TABLE OF CONTENTS
(Continued)

Transient stimulated Raman amplification in hydrogen

ABSTRACT

We describe the results of an extensive study of transient stimulated Raman scattering in hydrogen gas. Measurements of self-generation thresholds, conversion efficiency, and the dependence of small-signal amplification on pump energy and gas pressure are presented. Strong dependence of the amplification on the self-phase modulation of the pump and seed–Stokes pulses, on their relative time of arrival at the Raman amplifier, and on the seed-Stokes pulse asymmetry has been observed. The experimental measurements are compared with theoretical predictions that are based on extensions of published transient theories to take into account the spatial and temporal profiles of the pulses as well as their phase modulation. Excellent agreement with the theory, especially with regard to the scaling of the small-signal amplification with pump-pulse energy, is obtained when all of the specific characteristics of the pump and Stokes pulses are included in the calculations.

1. INTRODUCTION

Transient stimulated Raman scattering (SRS) occurs when the nonlinear polarization in the medium cannot respond completely during the pump pulse. It is generally encountered in stimulated scattering of picosecond pulses in gases and liquids and can also be important for longer pulses in gases under certain conditions. Here we report on an extensive study of transient Raman amplification in hydrogen gas. Our emphasis is on the properties of the amplified Stokes pulse relative to those of the incident Stokes pulse, in contrast to most of the work published elsewhere. To help in understanding the general properties of the Stokes amplification that are predicted by theory, we develop a number of approximate analytic results that give both time- and space-resolved and time- and space-integrated expressions for the amplified Stokes intensity. We report experimental measurements of Stokes amplification as a function of pump-pulse energy, gas pressure, and relative timing between the input Stokes and pump pulses. Phase-pulling effects are discussed and saturated-gain measurements are presented. Our results are compared with predictions of published theory and indicate where the theory is applicable and where a more complete analysis is required. We also demonstrate that the amplification is sensitive to the relative timing between the incident Stokes and pump pulses. Gain enhancements between 200 and 800 are observed for optimally timed pulses relative to that obtained with coincident pulses.

2. TRANSIENT RAMAN THEORY

Transient Raman scattering of plane waves in the absence of dispersion but with the ac-Stark shift of the levels involved in the Raman transition included is described by the equations

$$\partial A_S(r,z,t)/\partial z = i\kappa_2 A_L(r,z,t)\, Q^*(r,z,t) \tag{1a}$$

$$\partial A_L(r,z,t)/\partial z = i\kappa_2(\omega_L/\omega_S)\, A_S(r,z,t)\, Q(r,z,t) \tag{1b}$$

$$\partial Q^*(r,z,t)/\partial t + [-i(\omega_0 - (\omega_L - \omega_S) - \Delta_1 |A_L|^2 - \Delta_2 |A_S|^2) + \Gamma]\, Q^*(r,z,t) = -i\kappa_1 A_L^*(r,z,t)\, A_S(r,z,t) \tag{1c}$$

where $\kappa_2 = (4\pi N\omega_S/n_S c)\,\partial\alpha/\partial Q$, $\kappa_1 = (1/2\omega_0)\,\partial\alpha/\partial Q$, ω_0 is the frequency of the material excitation, $\partial\alpha/\partial Q$ is the derivative of the molecular polarizability with respect to the normal coordinate of the active mode, N is the number density of the molecules, ω_S is the Stokes frequency, n_S is the refractive index at the Stokes frequency, and Γ is the linewidth of the Raman transition, which is equal to the inverse of the dephasing time T_2. These equations have been written in a reduced coordinate system that moves with the pulse. The position, z, and time, t, coordinates are related to the laboratory position and time coordinates by $z = z_{lab}$, and $t = t_{lab} - z_{lab}/c$. We have also allowed the fields to depend on the transverse coordinate r to account for beam profiles, but we have neglected diffraction of transverse structure. The equations are therefore valid in the collimated beam approximation.

The field amplitudes in Eqs. (1) are defined by their relations to the total electric and phonon fields defined as

$$E_{L(S)}(r,z,t) = 1/2\left[A_{L(S)}(r,z,t)e^{i(k_{L(S)}z - \omega_{L(S)}t)} + A^*_{L(S)}(r,z,t)e^{-i(k_{L(S)}z - \omega_{L(S)}t)}\right]$$

$$Q(r,z,t) = 1/2\left[Q(r,z,t)e^{i(k_0 z - \omega_0 t)} + Q^*(r,z,t)e^{-i(k_0 z - \omega_0 t)}\right]$$

The variables in Eqs. (1) are thus the amplitudes of the real fields.

The Stark shift coefficients Δ_1 and Δ_2 are given by

$$\Delta_1 = \frac{1}{4\hbar^2} \sum_i \left\{ \frac{|\mu_{2i}|^2}{\omega_{io} + \omega_S} - \frac{|\mu_{0i}|^2}{\omega_{io} - \omega_L} \right\}$$

$$\Delta_2 = \frac{1}{4\hbar^2} \sum_i \left\{ \frac{|\mu_{2i}|^2}{\omega_{io} - \omega_L} - \frac{|\mu_{0i}|^2}{\omega_{io} + \omega_S} \right\}$$

where μ_{0i} and μ_{2i} are transition dipole moments connecting states i with the ground state and the final state of the Raman transition, respectively.

The variable Q in Eqs. (1) is the normal-mode coordinate of excitation of a single molecule and is independent of the density N. This choice allows a direct identification with the Raman equations as derived from the density matrix, which allows in turn a straightforward introduction of the Stark shift terms.

Transient scattering is important when the time variation of the pump pulse is comparable to, or faster than, T_2, so that the time derivative in Eq. (1c) cannot be neglected. Formal solutions for the Stokes field amplitude and the material excitation have been given in the literature under the assumption of low pump depletion, no initial phonon population, and neglecting the ac-Stark shift. These solutions have the form:

$$A_S(r,z,t) = A_S(r,0,t) + (\kappa_1\kappa_2 z)^{1/2} A_L(r,t)$$

$$\times \int_{-\infty}^{t} e^{-[\Gamma(t-t')]} A_L^*(r,t') A_S(r,0,t') \; I_1[2\{\kappa_1\kappa_2 z [\tau(r,t) - \tau(r,t')]\}^{1/2}] \; [\tau(r,t) - \tau(r,t')]^{-1/2} \, dt' \quad (2a)$$

$$Q^*(r,z,t) = -i\kappa_2 \int_{-\infty}^{t} e^{-[\Gamma(t-t')]} A_L^*(r,t') A_S(r,0,t') \; I_0[2\{\kappa_1\kappa_2 z [\tau(r,t) - \tau(r,t')]\}^{1/2}] \, dt' \quad (2b)$$

where

$$\tau(r,t) = \int_{-\infty}^{t} |A_L(r,t')|^2 dt' \quad (3)$$

is proportional to the integral of the pump intensity up to time t and $I_n(x)$ is the modified Bessel function of the first kind of order n.

In the extreme transient regime ($t \ll T_2$) the general properties of these solutions are that the gain peaks near the tail of the pump pulse, it is independent of the linewidth Γ, and

the maximum gain is less than the steady state gain for a pulse with the same peak pump intensity. In addition, the gain depends only on the integrated pump energy and not on the pump intensity. Steady state behavior is reached after a time $t_{ss} = G_{ss}T_2$, where $G_{ss} = 2\kappa_1\kappa_2|A_L|^2z/\Gamma$ is the steady state gain that would be obtained with a pump pulse of amplitude A_L if it lasted long enough. For most situations, which involve Raman amplification with significant gain, we can expect that t_{ss} will be at least one order of magnitude greater than T_2 and, for the very high intensities that are normally used in SRS with picosecond pulses, it can easily exceed T_2 by three or more orders of magnitude.

3. EXPERIMENTAL MEASUREMENTS

A. Experimental Apparatus

We have made measurements of transient amplification and saturation using second-harmonic radiation from a Nd:YAG mode-locked laser for both vibrational and rotational scattering. A schematic of the experimental apparatus is shown in Fig. 1.

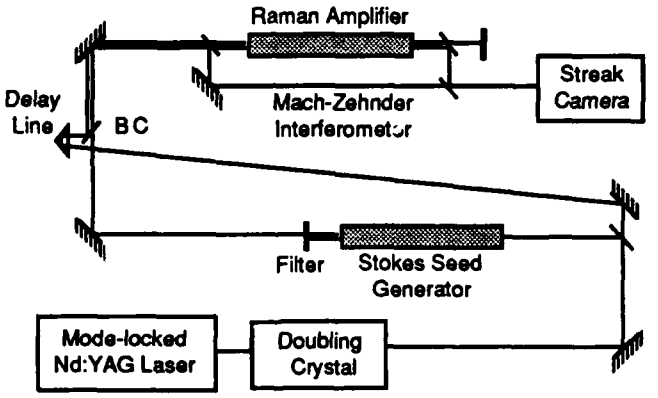

Figure 1. Schematic diagram of the experimental arrangement. The arrangement shown was used for the transient vibrational-Stokes gain measurements using linearly polarized light. Additional optics were added for producing circularly polarized light for use with rotational–Stokes amplification (see text). The seed-Stokes beam was not used for the self-generation measurements. PD indicates photodiodes used for pulse inergy measurements.

A single 40-psec pulse was switched out from the oscillator pulse train and amplified, first in a 1/4 inch diameter rod and then in a 3/8 inch diameter rod, producing output pulses at 1.06 μm with energies of the order of 20 - 40 mJ. The beam was spatially processed between the

two amplifiers to provide a truncated Airy disc at the second amplifier to minimize distortions due to self-focusing in the amplifier rod. The output pulse was then frequency doubled in a two inch long KDP crystal with a conversion efficiency approaching 50%, giving 10 - 20 mJ of radiation at 532 nm in a pulse that followed the temporal profile of the fundamental.

The 532 nm laser beam was then divided into two parts with a beamsplitter to provide 80% of the pump radiation for the Raman amplifier and 20% to drive a single-pass self-generator that provided the seed-Stokes radiation. The seed-Stokes generator consisted of a 100-cm-long cell filled with H_2 gas at pressures between 2 and 100 atm. The pump radiation for the seed Stokes was gently focused into the generator to minimize production of second and higher order Stokes. The seed generator was operated well into saturation to provide a seed pulse that was as close to the pump pulse in temporal and spatial extent as possible. The output at the first vibrational Stokes wavelength was separated from the pump by a color filter and was then spatially filtered. It typically had about 5 μJ of energy after the spatial filter. Other experiments, which were done using the rotational Stokes wavelength, required two narrow-band interference filters in place of the single color filter used for the vibrational measurements.

The remaining 80% of the pump radiation was also spatially filtered and passed through a variable delay path to allow adjustment of the relative timing between the pump and seed-Stokes pulses at the Raman amplifier. The pump and seed-Stokes beams were combined with a dichroic mirror and then telescoped to beam waist sizes (1/e field radius) of ω_0=0.61 and 0.48mm for the Stokes and pump beams, respectively, as determined by measurements with a diode array. The corresponding confocal parameters of b=340 cm and 270 cm were both well in excess of the 100 cm length of the amplifier cell that was used for these experiments. The gain of the amplifier was controlled by varying the pump pulse energy with calibrated, nonwedged, neutral-density glass filters or by changing the gas pressure. The Raman seed generator and amplifier cells were connected to a common fill line to ensure equal pressures in both cells so that the seed-Stokes was at the center of the gain line in the Raman amplifier.

Measurements of amplification for both vibrational and rotational scattering are reported in this paper. For the vibrational measurements, the pump radiation and the seed-Stokes light were linearly polarized parallel to each other as provided by the laser. For the rotational measurements, the seed-Stokes and pump beams were circularly polarized with opposite senses. The seed Stokes was generated with a circularly polarized pump beam and was subsequently converted to linear polarization orthogonal to the pump polarization. The orthogonally-polarized pump and seed-Stokes beams were then passed through the same λ/4

wave plate before the amplifier to produce beams with opposite circular polarization for the Raman interaction. The optics used for producing the circular polarizations are not shown in Fig. 1 for the sake of simplicity.

The input and transmitted Stokes and pump pulses were measured with fast photodiodes for determining relative pulse energies. Calibrated energy meters were used for absolute pulse energy measurements, and a 2-psec resolution streak camera was used for temporally resolved measurements. Amplification measurements as a function of pump pulse energy were obtained automatically with a microcomputer-based data-acquisition system using the photodiode measurements of the input and output Stokes pulses and pump pulses. The photodiode signals, which had a duration of 1 nsec due to the inherent characteristics of the photodiodes, were linearly amplified and stretched in time to have a duration of 2 μsec. The stretched pulses were registered in fast sample-and-hold units, which were then read through an analog-to-digital converter unit and computer processed. The energy meter signals also had to be amplified but could be read by relatively slow sample-and-hold units. The shot-to-shot energy variations in the laser allowed us to measure the amplification over a small range of pump energies while the neutral density filters were used to provide a wide range of pump energies. The microcomputer-based data acquisition program also was capable of restricting the pump pulses used to ones within an arbitrary percentage of a given energy. This feature was useful when measuring amplification as a function of pressure at constant pump energy.

Temporal profiles of the seed-Stokes and pump pulses are shown in Figs. 2(a) and 2(b), respectively. The pump pulse typically had a duration [full-width half-maximum (FWHM)] of 40 psec. The seed Stokes was asymmetric with a fall time that matched that of the pump and a rise time that was two to three times faster. The seed Stokes was generated in the second half of the pump pulse, as expected from theory, with a duration (FWHM) typically of the order of 25 psec.

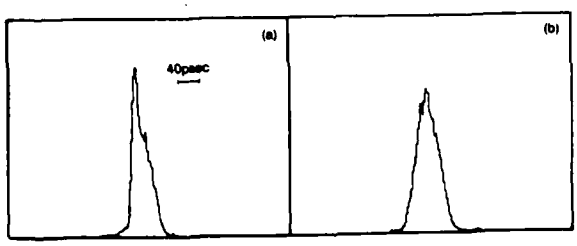

Figure 2. Temporal profiles of the seed-Stokes beam (a) and the input pump beam (b). The rise time of the seed Stokes is two to three times faster than its fall time.

The pump pulse exhibited self-phase modulation due to the nonlinear index of the Nd:YAG amplifier rods when the laser was operated at the intensities used for these experiments. The degree of self-phase modulation on the pump and seed Stokes was investigated both spectroscopically, using a 1-m spectrograph and an optical multichannel analyzer, as well as interferometrically, using a temporally-resolved Mach-Zehnder interferometer. Time-dependent interference patterns were obtained by imaging the vertical fringes produced by the interferometer across the horizontal slit of a 2-psec resolution streak camera.

Typical time dependent fringe patterns obtained from interferometer measurements of the pump beam are shown in Fig. 3. The straight-fringe pattern in Fig. 3(a) was obtained with equal path lengths in the interferometer arms. The patterns in Figs. 3(b) and 3(c) were obtained when one arm of the interferometer was delayed by 12 psec and 24 psec, respectively. The curvature of the fringes indicates that the temporal variation of the phase of the delayed arm does not match that of the reference arm. The "s" pattern shown in Fig. 3(b) is characteristic of that caused by self-phase modulation. When the pulse in one arm is delayed sufficiently far that its peak overlapsec the low intensity wing of the other, as in Fig. 3(c), the maximum fringe shift is determined by approximately twice the peak self-phase modulation. Measurements of the type shown in Fig. 3(c) indicated a maximum shift of between 1 and 1.5 fringes, corresponding to a peak self-phase-modulation depth between π and $1.5\,\pi$. The exact degree of self-phase modulation varied somewhat from shot-to-shot depending on the actual laser intensity.

Similar measurements of the seed-Stokes phase structure are shown in Fig. 4. The arms of the interferometer were equal for the measurements in Fig. 4(a), while one arm was delayed by 16 psec for the measurements in Fig. 4(b). Again the fringe pattern is straight for the measurements with the balanced interferometer but shows bending when the path lengths in the two arms are different. The fringe bending of the Stokes beam is much less than that observed with the pump beam because the seed Stokes is generated in the tail of the pump. As a result, it carries only the phase excursion characteristic of the tail of the pump, rather than the larger phase-excursion characteristic of the full pump.

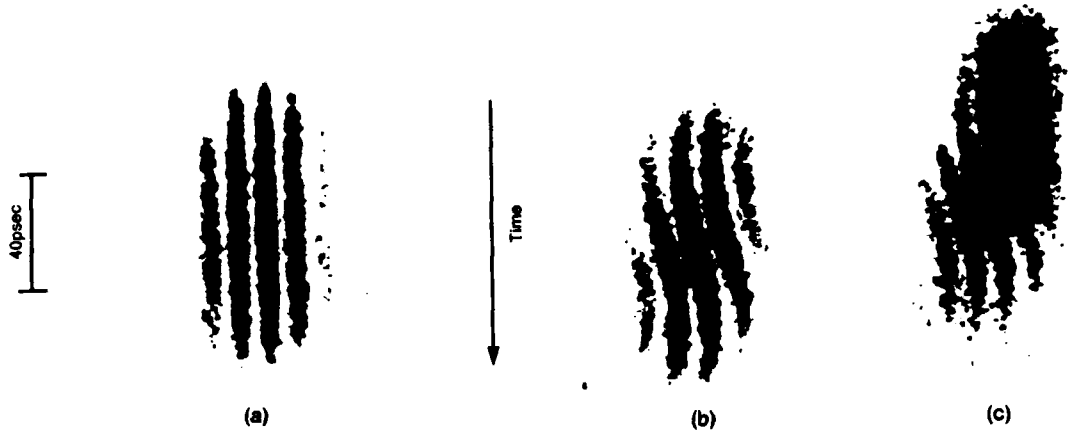

Figure 3. Interference fringes obtained with the 532 nm pump beam using the time-resolved Mach-Zehnder interferometer. The path lengths of the interferometer arms were equal in (a), and the reference arm was delayed by 12 psec in (b) and 24 psec in (c). The curvature of the fringes in (b) and (c) is due to self-phase

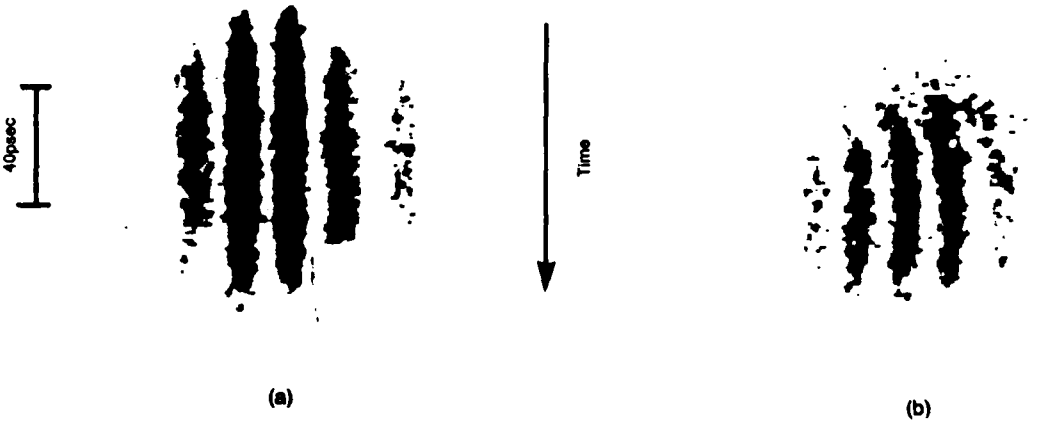

Figure 4. Interference fringes obtained with the seed-Stokes beam using the time-resolved Mach-Zehnder interferometer. The path lengths of the interferometer arms were equal in (a), while the reference arm was delayed by 16 psec in (b). The curvature of the fringes in (b) is due to self-phase modulation.

The time-integrated spectrum of the pump pulse, shown in Fig. 5(a), exhibits a double peaked structure that is also characteristic of self-phase-modulated pulses. The depth of the trough between the peaks is consistent with a peak self-phase modulation between π and 1.5 π, in agreement with the time dependent interferometer data of Fig. 3. The time integrated spectrum of the seed-Stokes pulse is shown in Fig. 5(b). The spectrum has only a single peak and is offset in frequency from the central value expected from the center laser frequency. This behavior is consistent with the smaller peak self-phase modulation observed in the Stokes interferometer measurements (Fig. 4(b)) together with the fact that the seed Stokes is generated in the tail of the pump where the self phase modulation causes an upshift in the pump frequency.

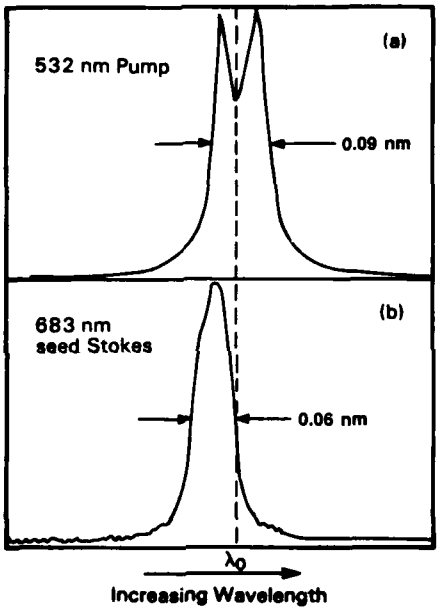

Figure 5. Spectroscopic profiles of the pump (a) and the seed-Stokes beams (b), showing the self-phase-modulation of between π and 1.5π carried by the pump. The seed Stokes, which is generated in the tail of the pump pulse, shows a smaller phase modulation and a spectral offset from the center frequency expected in the absence of self-phase modulation.

B. Experimental Results

Measurements of the amplification for both the vibrational and rotational Stokes were made as a function of pump energy, showing very similar behavior in the two cases. Typical results for the vibrational-Stokes amplification are shown in Fig. 6 for three different ratios of seed-Stokes to pump energy. At a given seed-Stokes energy, the amplification rises rapidly

until the onset of pump depletion, after which the amplification becomes approximately linear with pump energy. The point at which pump depletion occurs changes depending on the amount of amplification the incident Stokes input can be given before it becomes a significant fraction of the pump energy. This effect is seen in all three curves in Fig. 6. Saturation effects are apparent in the experimental measurements when the amplified Stokes energy is larger than about 1.6% of the input pump energy. This value agrees with numerical calculations that showed evidence of pump depletion when the amplified Stokes energy exceeded 1% of the initial pump energy.

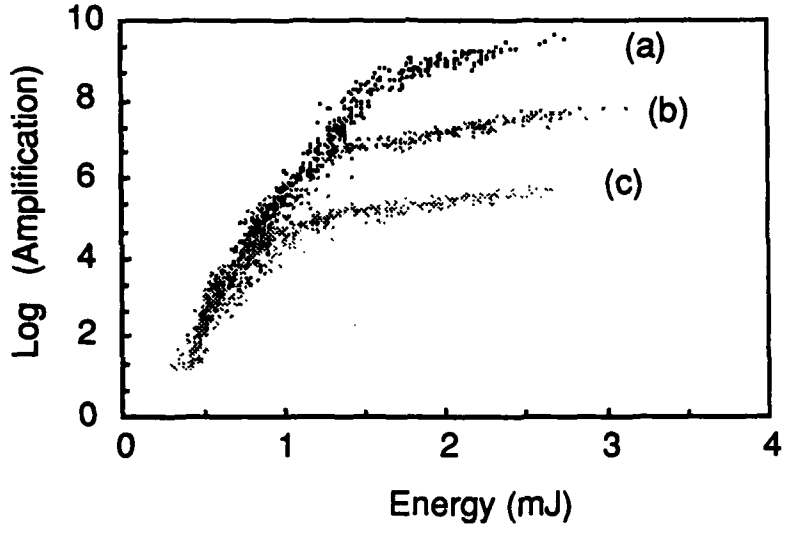

Figure 6. Dependence of the vibrational-Stokes amplification on pump pulse energy at a H_2 pressure of 30 atmospheres for ratios of the seed-Stokes energy to pump energy of 10^{-10}:1 (a); 10^{-8}:1 (b), and 10^{-6}:1 (c).

1. Pump-Depletion Measurements

The highest stable small-signal amplification measured in our experiment, obtained with a seed-Stokes-to-pump-energy ratio of 10^{-9}, was e^{19} (2×10^8). Self-generation occurred when the pump energy was increased by about 20% over that required to give the gain of e^{19}, indicating a self-generation energy-amplification threshold of approximately e^{23}, or 10^{10}.

Both conversion efficiency and temporal pulse shapes were studied in the high pump depletion regime. The highest consistent energy-conversion efficiency measured was 58% and occurred when the input seed-Stokes pulse had an energy that was approximately 1% of the input pump pulse energy. This value corresponds to a 75% photon conversion efficiency. The temporal shapes of the amplified Stokes and the depleted pump pulses were measured

with the 2 psec resolution streak camera. A typical measured temporal distribution for a depleted pump pulse is shown in Fig. 7(b). The H_2 pressure for this interaction was 20 atm, and the ratio of the input pump to seed-Stokes energy was 200 to 1. The depleted pump pulse shows a series of decreasing oscillations. Similar oscillations have been discussed theoretically and have previously been observed using nanosecond-duration pulses. [10] No oscillations, however, have previously been reported in the highly transient limit.

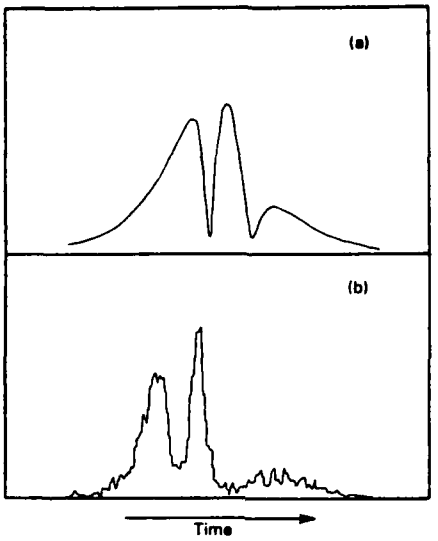

Figure 7. Theoretical (a) and experimental (b) temporal pulse shapes of the depleted pump.

A theoretical distribution of a depleted pump pulse is shown in Fig. 7(a). The theoretical calculation included ac-Stark-shift effects due to the high electric fields present in the medium and was performed by numerically integrating Eqs. (1) directly. The calculation was performed with a level of depletion sufficient to give three peaks in the depleted pump pulse. At this level of depletion the agreement between the experimental and theoretical distributions is quite good.

The oscillations on the depleted pump pulse can be understood by considering the energy flow between the Stokes, pump, and phonon fields as described by Eq. (1). As the Stokes and phonon fields grow large, the pump field is driven toward zero. Since the phonon responds slowly during the pulse, the pump phase eventually reverses sign, resulting in a flow of energy back into the pump. More oscillations follow if the depletion level is large enough.

The ac-Stark effect has to be included in the theoretical calculation to obtain good agreement between calculated curves and experimental data at the oscillating-pump-amplitude minima. Without the ac-Stark effect the calculated depleted pump amplitude is

driven completely to zero between peaks. Experimentally the pump amplitude always stays above zero, indicating that the ac-Stark effect is important in this highly depleted pump regime.

2. Small-Signal Gain Measurements

We have measured the Stokes amplification in the small-signal regime as functions of the gas pressure, the relative timing between the seed-Stokes and pump pulses, and the pump energy.

a. Pressure dependence. The dependence of the vibrational-Stokes amplification on the H_2 pressure over the range of 7–100 atm is shown in Fig. 8 for three different values of the pump energy. The highest pump energy density was of the order of 400 mJ/cm^2 (curve a), and decreased from curve (a) to curve (c) in the ratios of 1:0.59:0.37. Similar measurements for the rotational-Stokes amplification are shown in Fig. 9. In both cases the variation of the Stokes amplification with pressure is very similar to the variation of the small-signal Stokes amplification with pump energy that will be discussed in Sec. 3B2d. This similarity indicates that the amplification scales as the product of density and pump energy, as expected from theory.

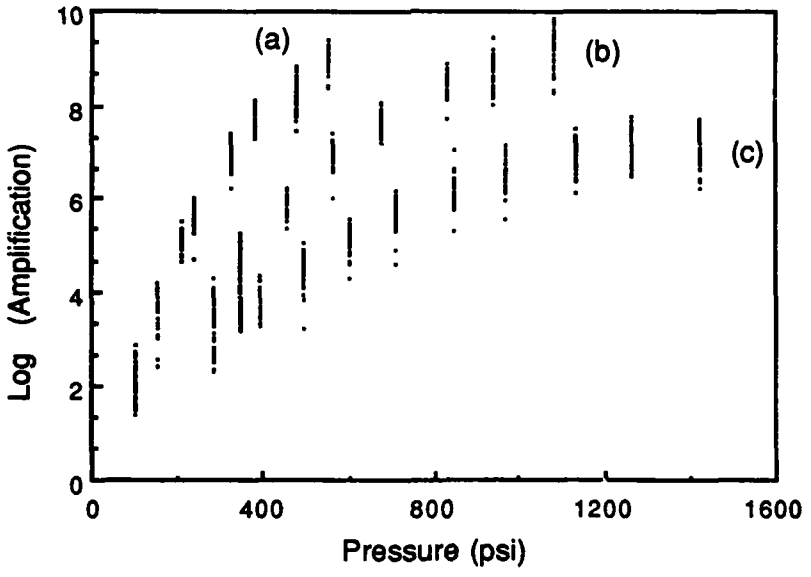

Figure 8. The dependence of the vibrational-Stokes amplification on the pressure of H_2 for pump energies of 400 mJ/cm^2 (a), 237 mJ/cm^2 (b) and 148 mJ/cm^2 (c).

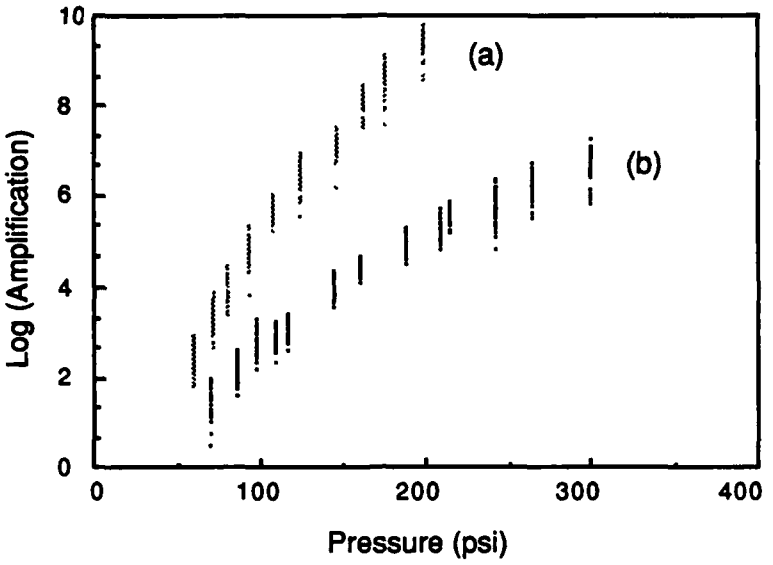

Figure 9. The dependence of the rotational-Stokes amplification on the pressure of H_2 for two different pump energies.

The increase of the small-signal amplification with pressure in the range greater than 10 atm can be contrasted with the behavior expected for the gain in the steady state. Under steady state conditions the gain becomes independent of pressure above about 10 atm because pressure broadening of the Raman line offsets increases due to higher density. In the present situation the fact that the gain continues to increase as a function of pressure above 10 atm reflects the transient nature of the interaction in which the gain retains a dependence on density, but not on linewidth.

b. Phase pulling. The phase modulation exhibited by the amplified Stokes pulse was investigated both spectrally and interferometrically and shows that the phase of the amplified Stokes is pulled into correlation with that of the pump pulse. For these measurements the same temporally-resolved Mach-Zehnder interferometer described in Sec. 3A was used at the Stokes wavelength. The signal arm of the interferometer passed through the Raman amplifier, while the reference arm passed outside it. Measurements of the time-dependent fringe pattern, shown in Fig. 10, were made with and without the amplifier pumped, with equal and unequal path lengths in the interferometer arms, and with various

relative timings between the pump and seed-Stokes pulses. The relative path delay of the interferometer was varied in discrete steps by placing uncoated quartz flats in one or the other of its two arms.

When the path lengths in the two interferometer arms were equal and the Raman amplifier was unpumped, the fringe pattern was straight (Fig. 10(a)) as would be expected. The pattern shown in Fig. 10(b) was obtained when the interferometer arms had equal path lengths, the amplifier was pumped, and the seed Stokes was advanced relative to the pump by approximately 25 psec. This timing corresponded to the condition for optimal conversion as will be discussed in the next section. In this situation the reference Stokes, which carries the phase signature of the tail of the pump where it was created, interferes with that part of the signal Stokes that is amplified by the leading edge of the pump. The curvature of the fringes indicates that the temporal variation of the phase of the amplified Stokes pulse does not match that of the reference Stokes, even though the optical path delay in the two interferometer arms is equal. The fringe pattern shown in Fig. 10(c) was obtained when the Stokes reference arm was delayed by 26 psec to match the relative delay of the pump and when the Raman amplifier was pumped. In this situation the Stokes reference interferes with the part of the signal Stokes that is amplified by the trailing edge of the pump. The straight fringes observed under this condition indicate that the phase of the Stokes pulse that is amplified by the trailing edge of the pump is correlated with the phase of the Stokes pulse that was created in the trailing edge of the pump. This result can be contrasted with that shown in Fig. 4(b) in which the Stokes fringes showed curvature when the interferometer arms were unbalanced but the Raman amplifier was unpumped. The straight fringes obtained when the Raman amplifier is pumped indicate that the Stokes phase has been pulled into correlation with the pump.

This conclusion was verified with measurements taken with the interferometer arms balanced, but with the seed-Stokes pulse delayed relative to the original timing by about 30 psec. In this situation the signal Stokes is amplified by the trailing edge of the pump, the same region of the pump in which the seed Stokes was created. Again straight fringes were observed (Fig. 10(d)), indicating that the signal Stokes remains correlated with the reference Stokes, and that, therefore, there is no phase pulling when the seed Stokes is amplified by the part of the pump in which it was created.

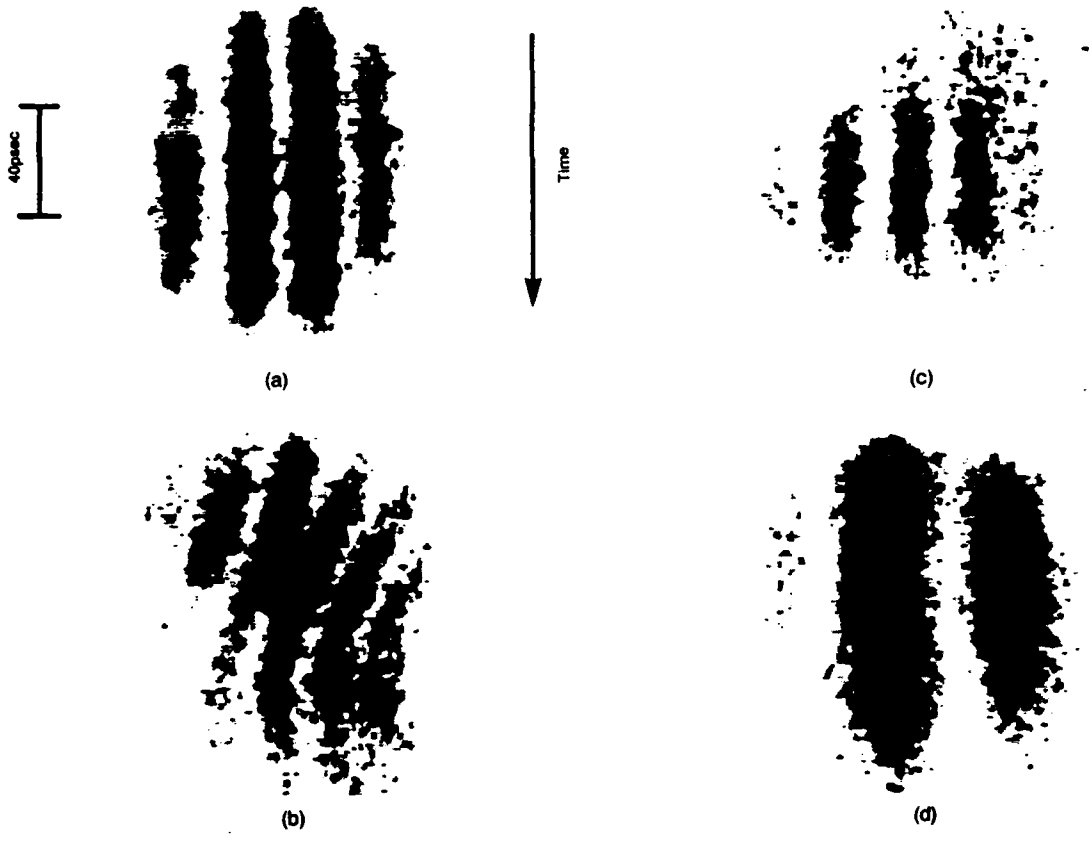

Figure 10. Time dependent interference patterns of the amplified and reference Stokes beams under various conditions: (a), balanced interferometer arms, unpumped amplifier; (b), balanced interferometer arms, pumped amplifier, seed-Stokes pulse advanced by 25 psec relative to the pump; (c), Stokes reference arm delayed by 26 psec, amplifier pumped, seed-Stokes pulse advanced by 25 psec relative to the pump; and (d), balanced interferometer arms, amplifier pumped, seed-Stokes pulse delayed by 5 psec relative to the pump.

The conclusion that the Stokes phase is pulled into correlation with the pump was further confirmed by comparison of the pump and amplified-Stokes spectra as shown in Fig. 11. Although the spectrum of the seed Stokes showed a single-peaked distribution offset from the expected central frequency (Fig. 5(b)), the spectrum of the amplified Stokes (Fig. 11(b))

shows a double peaked structure similar to that seen in the spectrum of the pump radiation (Fig. 11(a)). The depth of modulation of the amplified-Stokes spectrum is consistent with a peak self-phase modulation of the order of π, the same value obtained for the peak phase modulation of the pump pulse.

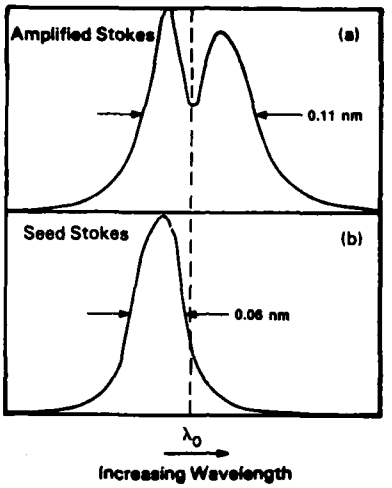

Figure 11. Spectral profiles of the amplified and seed-Stokes pulses. The profile of the amplified Stokes matches that of the pump (Fig. 5(a)) while that of the seed Stokes does not, indicating that the amplified Stokes is pulled into correlation with the pump.

The degree of phase pulling experienced by the Stokes pulse at its optimal timing advance of 25 psec was also examined as a function of the total gain of the amplifier. These measurements showed that the phase pulling was complete for amplifications above about ten.

c. Pulse timing. We have measured the effect on the amplification of the relative timing between the seed-Stokes pulse and the pump pulse. A schematic of the interaction is shown in Fig. 12. The time difference between the peak of the pump pulse and the peak of the Stokes is defined as Δ, with Δ positive when the seed-Stokes pulse arrives earlier than the pump. The experimentally observed variation of the vibrational-Stokes amplification with pump energy for different values of Δ is shown in Fig. 13.

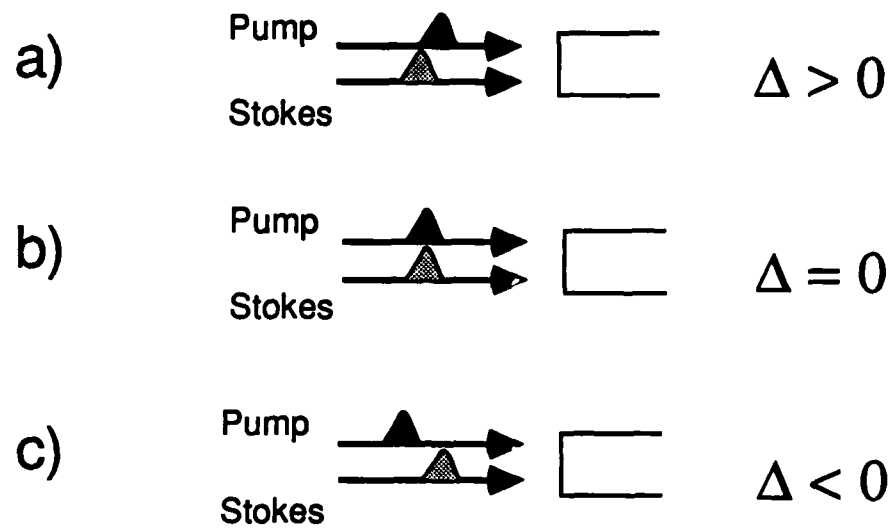

Figure 12. Schematic diagram of the relative timing of the seed-Stokes and pump pulses. The quantity Δ represents the time interval between the arrivals of the peaks of the seed-Stokes and pump pulses at the input plane of the amplifier cell. Positive Δ corresponds to cases in which the seed-Stokes pulse leads the pump pulse in time.

Generally speaking, the gain shows the same type of behavior as a function of pump energy at different values of Δ. As Δ is varied, however, the magnitude of the gain at a given pulse energy changes. In addition, the slope flattens as Δ is decreased, an effect that is related to the phase-pulling discussed in Sec. 3B2b. These measurements show that there is an optimal timing of the seed-Stokes pulse relative to the pump pulse for providing maximum gain. This behavior is shown graphically in Fig. 14, where the dependence of the vibrational-Stokes amplification on pulse timing at constant pump energy is displayed. The amplification peaks when the seed-Stokes pulse is advanced by about 20 psec relative to the peak of the pump pulse, with a gradual falloff for larger advances and a steeper falloff as the advance is decreased. At the optimal timing advance the Stokes amplification was about 400 times greater than it was when the seed-Stokes and pump pulses arrived together.

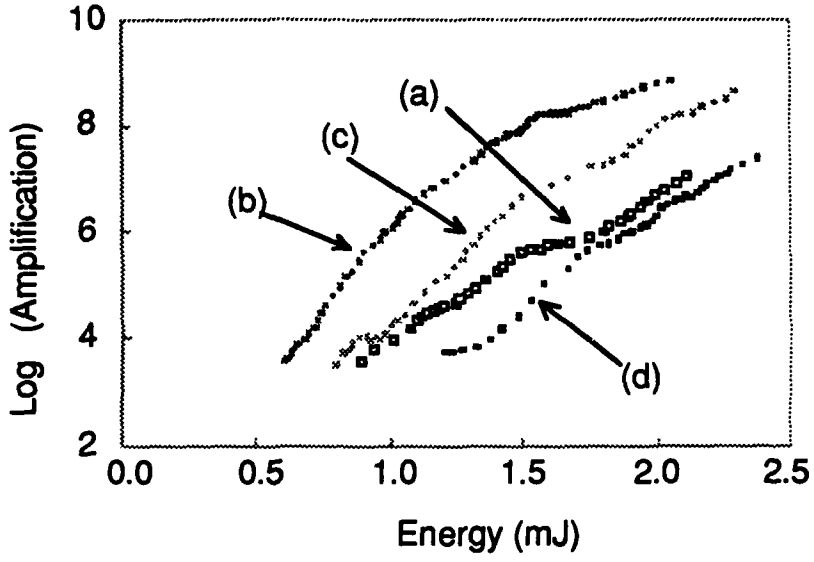

Figure 13. The variation of the Stokes amplification with pump energy for different relative timings, where the time difference between the peak of the pump pulse and the peak of the Stokes is defined as Δ. Δ is positive when the seed-Stokes pulse arrives earlier than the pump. Curve (a) shows the case where the pump and seed Stokes are essentially overlapped and reflects relatively little phase pulling. Curve (b) shows the peak gain obtained at optimum timing when Δ=20 psec. Curve (c) corresponds to Δ=70 psec, and curve (d) corresponds to Δ=88 psec.

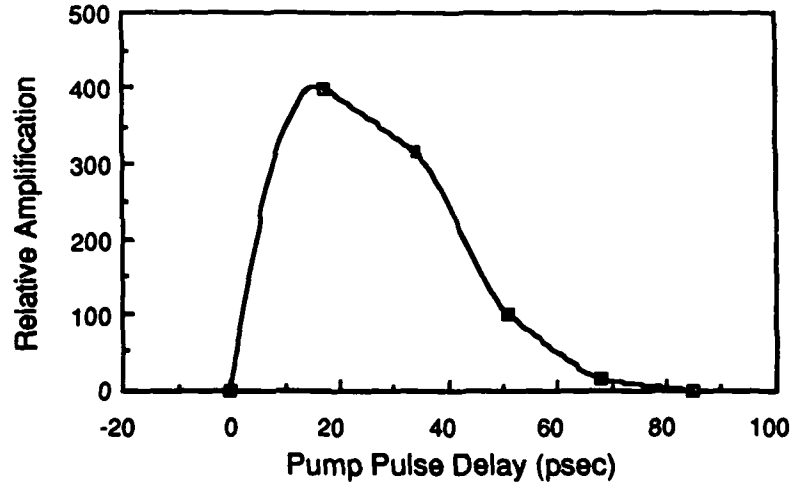

Figure 14. The experimentally observed variation of the small-signal vibrational-Stokes amplification for different values of pump pulse delay. The maximum amplification was about 5×10^8.

Similar behavior was observed in the rotational-Stokes amplification as shown in Fig. 15. Again the optimal time of arrival for the seed-Stokes pulse is about 20 psec before the peak of the pump. The observed enhancement of the amplification at optimal timing relative to that at coincident timing was of the order of 800. In addition the variation of the amplification shows a plateau for timing advances greater than the optimal.

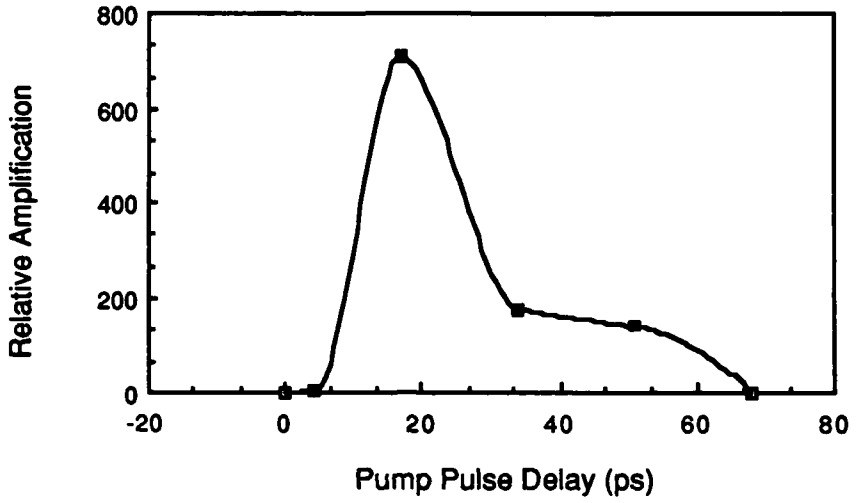

Figure 15. The experimentally observed variation of the small-signal rotational-Stokes amplification as a function of pump pulse delay. The maximum amplification was about 5×10^8.

The dependence of the amplification on the relative timing of the seed-Stokes pulse and the pump pulse can be understood by considering the origin of the reduced gain in the transient regime. The spatial rate of growth of the Stokes pulse [Eq. 1(a)] depends on the instantaneous product of the pump and the phonon amplitudes, while the phonon amplitude depends upon the integral of the product of the Stokes and pump fields [Eq. 1(c)]. The phonon amplitude thus builds up slowly during the pump pulse, peaking towards the rear, and the Stokes amplitude growth rate is reduced relative to the steady state because the pump amplitude is high when the phonon amplitude is low and vice versa. When the Stokes pulse is brought in ahead of the peak of the pump, the phonons can start building up sooner, resulting in a larger phonon amplitude near the peak of the pump pulse and consequently a larger overall gain.

We would expect that the increase in gain should be dependent on the temporal profile and duration of the Stokes pulse relative to the pump pulse. A relatively large increase would be expected if the Stokes pulse has a relatively sharp peak, encouraging rapid growth of the phonons when the Stokes pulse is properly advanced, and a sufficiently strong trailing tail to provide energy to be amplified near the peak of the pump pulse. Such a situation could occur if the Stokes pulse is shorter than the pump or if it is asymmetric, with a fast rise and a slower fall as existed in our experiments. In contrast, if both the Stokes and pump pulses have square temporal profiles the gain would be expected to be maximized when the pulses were coincident.

We have examined these effects theoretically byusing numerical evaluations of the integral in Eq. 2(a) for the Stokes-field amplitude and integrals over spatial and temporal profiles to allow comparison with our measurements. We used both Gaussian and hyperbolic-secant temporal pulse shapes for the pump and seed Stokes. We also considered symmetric and asymmetric pulses for the seed Stokes, seed-Stokes pulse durations that were equal to and shorter than the pump pulse duration, and various levels of peak self-phase modulation. An example of the theoretical prediction of time- and space-integrated amplification as a function of Stokes advance Δ for a hyperbolic-secant temporal pulse without self-phase modulation is shown in Fig. 16. The asymmetries chosen for these calculations, corresponding to rise times that are two and three times faster than the fall time, are approximately characteristic of the pulses used in the experiments. Calculations for a symmetric pulse are shown for comparison.

The qualitative trends just described are evident in the calculated results. The amplification is a maximum when the peak of the Stokes pulse arrives ahead of the peak of the pump by about 0.5 —1-pulse durations. The amplification falls off relatively rapidly for smaller advances and more slowly for larger advances in agreement with the experimental observations. The enhancement of the amplification at the optimal timing relative to that obtained when the peaks of the pulses were coincident depends on the degree of asymmetry, increasing as the seed-Stokes pulse becomes more asymmetric. The optimal timing is only weakly dependent on the seed-Stokes pulse shape. The value of the amplification at the optimal timing is relatively insensitive to the seed-Stokes asymmetry, but the amplification at coincident timing depends strongly on the Stokes pulse shape.

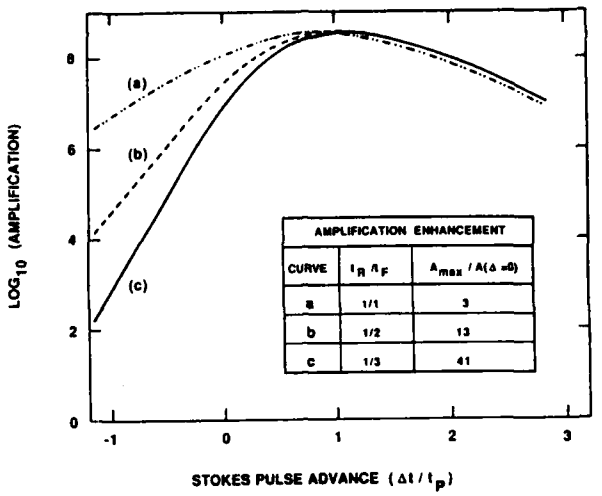

Figure 16. Theoretical dependence of the time- and space-integrated amplification on the Stokes-pulse advance for various ratios of the rise to fall time of the seed-Stokes pulse assuming a hyperbolic-secant amplitude distribution for the pump and Stokes pulses and no self-phase modulation.

Results of a similar calculation using an asymmetric pulse with a rise-to-fall-time ratio of 1:3 and a peak self-phase modulation of π are shown in Fig. 17. The variation of amplification now exhibits a shoulder for timing advances greater than the optimal value similar to that seen in the experimental measurements of Figs. 15 and 16.

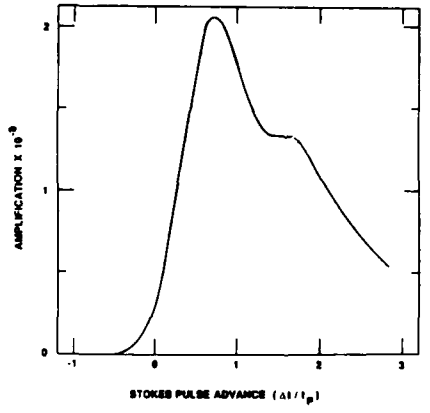

Figure 17. Theoretical dependence of the time- and space-integrated amplification on the Stokes-pulse advance for a rise to fall time ratio of 1:3, assuming a hyperbolic-secant amplitude distribution for the pump and Stokes pulses and a peak self-phase modulation of π. The phase modulation introduces a shoulder at large-pulse advances.

Additional calculations were done with pulses with Gaussian temporal profiles and with symmetric seed-Stokes pulses that were shorter than the pump. In each of these situations the amplification peaked when the Stokes pulse arrived before the pump. Our explanation, then, accounts for the qualitative features of our experimental observations. Comparison of theoretical results for various pulse shapes and asymmetries indicates that the detailed dependence of the amplification on the Stokes pulse advance and the numerical value of the enhancement at the optimal timing depends on the details of the pulse shape and degree of phase modulation, especially in the low intensity rising edge. In addition, the rapid variation of the amplification near zero timing advance for the asymmetric pulses can cause very large changes in the apparent gain enhancement for very small changes in the identification of the coincident timing. The experimentally observed gain enhancement could therefore be affected by our ability to identify accurately the coincident timing.

d. Dependence on pump energy. The small-signal amplification was measured extensively as a function of pump energy. A typical result for the vibrational Stokes is shown in Fig. 18. In obtaining these data care was exercised to ensure that the pump depletion was always below 1% so that the measured amplification would be in its small-signal limit. The data are presented on a graph that displays the log of the log of the amplification as a function of the log of the pump energy. Exponential variation of the amplification with pump energy would appear as a straight line, with the slope indicating the power law dependence of the exponent on the pump energy, while nonexponential behavior would be indicated by a curved line. When viewed over the five orders of magnitude that are displayed in Fig. 18, the amplification has a nonexponential dependence on the pump energy as discussed in Sec. 2. However, when viewed over restricted gain ranges, the amplification shown in Fig. 18 could be interpreted as having an exponential variation with pump energy with a power law dependence for the exponent between 0.7 and 1.5, depending on the level of amplification.

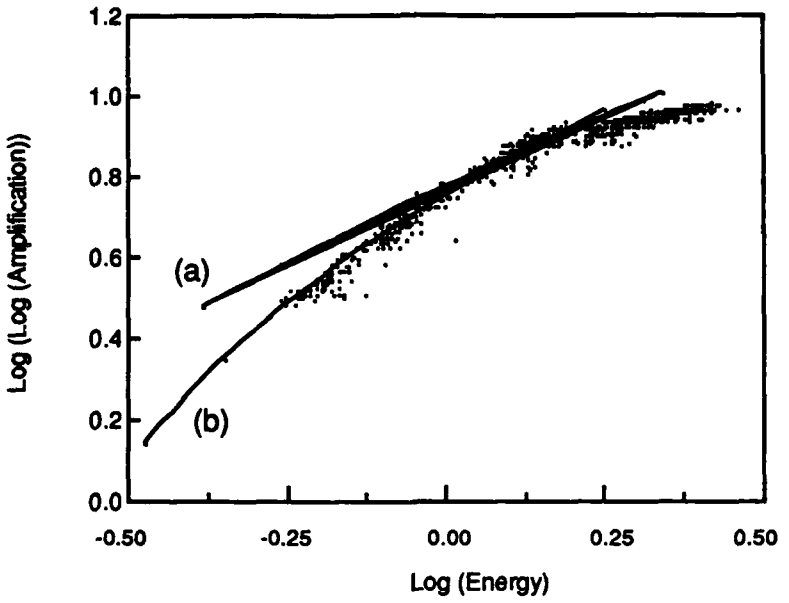

Figure 18. Experimental dependence of the vibrational-Stokes amplification on pump energy (points). Curve (b) was obtained by numerical evaluation of the integral in Eq. (2a), integrated over space and time, using seed-Stokes parameters appropriate to our experiment including pulse asymmetry, timing advance and self-phase modulation. Curve (a) was obtained with a similar calculation neglecting self-phase modulation.

We have compared the measured small-signal amplification with the predictions of the published theories. In making these comparisons between theory and experiment we have determined that all of the details associated with our measurements, such as seed-Stokes pulse asymmetry, timing advance, and degree of phase modulation, must be included in the theory. As a result the simplifying assumptions that lead to the analytic expression as discussed in Sec. 2 cannot be used. Rather, a full numerical evaluation of the integral in Eq. 2(a), using all of the appropriate seed-Stokes parameters, is necessary to explain our measurements.

Two theoretical curves are shown in Fig. 18. Each curve was obtained by integrating the calculated intensity amplification over space and time by using a hyperbolic-secant seed-Stokes pulse with a rise-to-fall-time asymmetry of 1:3, a Gaussian spatial distribution, and a timing advance of 0.85 pulse durations. Curve (a) was calculated without self-phase modulation, while curve (b) included self-phase modulation with a depth of π. In comparing the theoretical curves with the experimental data, adjustment was made along the horizontal

axis to obtain the best fit. This action compensates for systematic inaccuracies in absolute measurements of energy, beam size, and pulse duration. Because the vertical axis represents the ratio of two measured or calculated quantities, no adjustment was allowed along this direction. The calculation that included self-phase modulation (curve b) accounts for the observed scaling of amplification with pump energy very well. The calculation done without self-phase modulation, on the other hand, exhibits very poor agreement except at the very high end of the measurements.

The difference between the two theoretical curves is caused by the phase pulling, discussed in Sec. 3B2b, and occurs because of the combination of the self-phase modulation present on our pulses and the Stokes pulse advance necessary for optimal amplification. When the seed-Stokes pulse enters the amplifier it is not correlated with the pump since it is advanced with respect to the pump, and until it becomes correlated its gain is reduced. As a result the effective length of the amplifier over which full gain is experienced is reduced. At relatively low gains this can represent a significant fraction of the physical length of the amplifier. As the pump energy is increased the phase pulling is accomplished sooner, causing the amplification to increase because of both the increased pump energy and the larger effective amplifier length. The amplification that occurs with the self-phase-modulated pulse therefore increases faster with the pump energy than does the amplification of the pulse without phase modulation in the low gain region. At high gains only a small distance is required for phase pulling to correlate the pump and Stokes pulses, and the two theoretical curves eventually approach each other.

An example of the agreement between the theoretical and experimental scaling of amplification with pump energy for rotational scattering is shown in Fig. 19. Again all of the detailed parameters of the seed-Stokes and pump pulses, including the self-phase modulation, had to be included for the theory to agree with the experiment. When these parameters were included in the theory the agreement was again quite good.

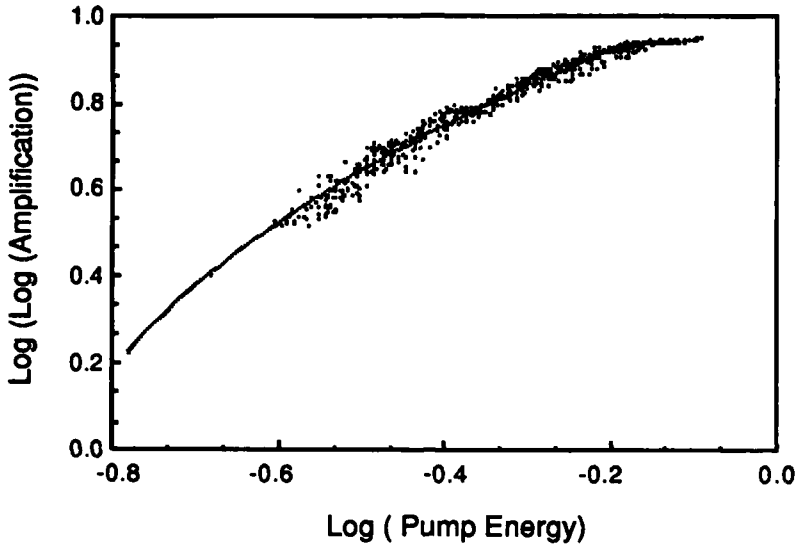

Figure 19. Experimental dependence of the rotational-Stokes amplification on pump energy (points). Curve (a) was obtained by numerical evaluation of the integral in Eq. (2a), integrated over space and time using seed-Stokes parameters appropriate to our experiment including pulse asymmetry, timing advance and self-phase modulation.

4. DISCUSSION AND SUMMARY OF TRANSIENT GAIN

We have presented measurements of transient Raman amplification for both vibrational and rotational shifts in H_2 gas in a range from small-signal gain to pump depletion. The small-signal gain has been measured as a function of pump energy and pressure, and the results are in substantial agreement with the transient theory when the relative timing of the pump and seed-Stokes pulses, the pulse shapes and asymmetries, the variations in the phase of the pump and seed-Stokes pulses, and integration over the spatial and temporal profiles of the pulses are included in the theory. In addition, a number of analytic expressions for the transient amplification of the Stokes intensity, energy, power, and energy density have been developed under certain restrictions, and approximate expressions for the moderate- to high-gain limits of those solutions have been presented. Phase pulling has been observed to occur in the amplified Stokes pulses to persist down to very low levels of amplification. Stable gains of e^{19} together with pump-depletion levels of 75% have been observed. Multiple oscillations have been observed on strongly depleted pump pulses, again in substantial agreement with theory. A strong dependence of the amplification on the relative timing of the pump and seed-Stokes pulses was reported for the first time.

This dependence has its roots in the transient buildup of the phonon population and is strongly dependent on the Stokes pulse shape, asymmetry, and duration relative to the pump pulse. Again results are in reasonable agreement with theoretical predictions, with exact agreement requiring inclusion of the detailed temporal and spatial profiles of the seed-Stokes and pump pulses, especially in the low-intensity rising edges.

The experimental and theoretical results indicate that the amplification does not follow a simple exponential dependence on the pump energy or gas pressure. However, over restricted ranges the amplification can be approximated by an exponential variation with a transient gain parameter u_m proportional to the quantity $(EN)^n$, where E is the pump energy, N the number density of the gas and n depends on the gain. For the measurements presented here, which covered amplifications from about e^5 to e^{19}, n varied between 1.5 and 0.7.

Quantum fluctuations in transient Raman amplification

ABSTRACT

We have investigated the pulse energy statistics in a transient stimulated Raman amplification experiment. Experiments were also performed using a self-generator, both in the chaotic linear regime and in the stabilized nonlinear regime. For an input seed-Stokes beam to control a transient, high gain Raman amplifier, operated near threshold, it must dominate the competing self-generated Raman which builds from quantum noise. Amplifier measurements have been made at a relative timing between the input seed-Stokes pulse and the pump, corresponding to that for optimal amplification where the seed Stokes precedes the pump. The measurements show the enhancement of the Stokes photons originating from noise due to the presence of the phonon field of the input seed Stokes. We have also measured the number of input seed-Stokes photons needed to produce a predominantly stabilized signature on the energy statistics of the amplified Stokes pulse. In addition, a near-field camera was used to record the spatial profiles of both the self-generated and the amplified Raman pulses. Three different Fresnel number (F#) systems have been investigated: (1) both the pump and the seed Stokes having F#0.8; (2) a pump pulse with F#1 and a seed-Stokes with F#2; and (3) a pump pulse with F#5and a seed-Stokes with F#10. The spatial mode of the larger Fresnel number system was found to heve a sharp threshold, with input Stokes energy, in switching from the random intensity patterns of the self-generated Stokes outputs, to the well-defined, uniform output more characteristic of a unity Fresnel number system. Also, the level of the input seed-Stokes pulse needed to reach this threshold for control of the large Fresnel number spatial mode is low ($2x10^3$ photons per mode) compared with the surprisingly large (10^9) number of input photons needed to establish a fully stabilized character in the unsaturated near unity Fresnel number Raman amplifier.

1. INTRODUCTION

The macroscopic fluctuations in the energy of individual pulses produced in a Raman self-generator have been observed experimentally and most of the features are contained within the quantum treatments which describe the buildup of stimulated Raman scattering from quantum noise in the linear regime. Photons of frequency ω_L scatter from a sample of ground state atoms leaving the atoms in an excited state and producing photons at the Stokes frequency ω_S, where the difference between ω_L and ω_S is a vibrational or rotational frequency of the Raman active medium. The first few photons at the Stokes frequency are emitted spontaneously, the actual number varying from pulse to pulse because of the

quantum noise initiation. The emission subsequently takes on a stimulated character as the pulse builds up in intensity to a level of the order of 10^9 photons. If there is no depletion of the laser pump field, or of the molecular population, then the statistical properties of the initiating photons are preserved. For a transient system, such that only one temporal mode exists, and for a Fresnel number $F=1$, (where $F = A/\lambda L$ with A the beam area, λ the wavelength and L the length of the pumped or generating volume) such that only a single spatial mode is sustained, the probability density function $P(W)$ for the Stokes energy W is a negative exponential

$$P(W) = \langle W \rangle^{-1} \exp(-W/\langle W \rangle)$$

where $\langle W \rangle$ is the mean value of the energy. In this case, the most probable energy is zero and 100% fluctuations about the mean are predicted. As the Fresnel number increases and more transverse modes are introduced, the quantum fluctuations are significantly reduced and the distribution of the total Stokes energy W_T is no longer described by a simple negative exponential, but instead is approximated by a gamma distribution

$$P_N(W_T) = \frac{1}{(N-1)!} \frac{W_T^{N-1}}{\langle W \rangle^N} \exp(-W_T/\langle W \rangle)$$

where $N (\propto F^2)$ is the number of statistically independent spatial modes. In the limit of a large number of spatial modes, the gamma distribution converges to a gaussian, as expected from the central limit theorem.

Experiments have also been done in the nonlinear regime where there was significant depletion of the pump energy and the theory of Mostowski-Raymer was extended to cover transient Raman scattering in a single spatial mode system with pump depletion. In contrast to the linear case, where the distribution of Stokes energies follows a negative exponential function, a well stabilized distribution of energies is found in the nonlinear regime, with a peak at the mean energy value of the Stokes pulse energy.

The primary purpose of the present work was to understand how a high gain, near threshold, Raman amplifier could be controlled by an input seed-Stokes beam. The seed Stokes beam, being derived from a self-generator driven into saturation, had a tight distribution of energies, whereas the pulse energy statistics of the unseeded Fresnel number 1 amplifier showed large intensity fluctuations. However, for a seeded amplifier in the unsaturated regime, the amplified pulse should have the identical statistical distribution as the original input seed Stokes pulse. Since we needed to know the amount of seed Stokes required to dominate the self-generated Raman, and since the spatial profiles of both outputs would appear Gaussian since the Fresnel number was small, a study of the statistical properties was essential. In the case of a large Fresnel number system the situation is more complicated, since the self-generator produces a spatial mode pattern with random

characteristics. Even for a Fresnel number 10 geometry, the statistical distribution of pulse energies for the self-generated Stokes was sufficiently different from that of the saturated input seed Stokes, having a mean energy value much les than 1, that the statistical character of the amplified Stokes in this larger aperture geometry was still a useful measure of the degree of control impressed upon the amplifier by the seed Stokes beam.

2. EXPERIMENT

The experimental apparatus used in these studies has been described above. In brief, a frequency-doubled Nd:YAG mode-locked laser with pulses of 40 psec duration and energies of 10 to 20 mJ at 532 nm was used both to produce the seed-Stokes pulse in a single-pass Raman self-generator and to pump the Raman amplifier. Both the seed-Stokes generator and the amplifier used H_2 gas at a common pressure in the range of 5 to 55 atm. The seed-Stokes generator was operated well into saturation with a depletion level of about 15% to assure a moderately stable seed-Stokes amplitude and the 682nm Stokes output was separated from the pump by use of a color filter. The seed-Stokes pulse typically had 15μJ of energy after spatial filtering and had a pulse duration of 25 psec with a rise time that was 2 to 3 times faster than that of the pump. The pump energy used in the Raman amplifier was also spatially filtered and was passed through a variable delay path to allow adjustment of the relative timing between it and the seed-Stokes pulse. There is an optimal timing of the seed-Stokes pulse relative to the pump pulse for providing maximum gain. The amplification peaks when the seed-Stokes pulse is advanced by about 20 psec relative to the peak of the pump pulse, with a gradual falloff for larger advances and a steeper falloff as the advance is decreased. The pump and seed-Stokes beams were combined and telescoped to a confocal parameter well in excess of the 100 cm length amplifier cell used for these experiments. The gain of the amplifier was controlled by varying the energy of the pump pulse while the degree of saturation could be adjusted by changing the energy of the seed-Stokes pulse incident in the amplifier

The input and transmitted Stokes and pump pulses were measured with fast photodiodes for determining relative pulse energies while calibrated energy meters were used for absolute pulse energy measurements. Histograms of output Stokes pulse energies were obtained automatically with a microcomputer-based data-acquisition system using the photodiode measurements of the input and output Stokes pulses and pump pulses. The photodiode signals, which had a duration of 1 nsec due to the inherent characteristics of the photodiodes, were linearly amplified and stretched in time to have a duration of 2 msec. The stretched pulses were registered in fast sample-and-hold units, which were then read through

an analog-to-digital converter unit and computer processed. The energy meter signals also had to be amplified but could be read by relatively slow sample-and-hold units. Acceptable shots were restricted to those with pump energies within a 5% or 1% range and histogram sample sizes were typically of 2000 laser pulses distributed into 100 bins.

The spatial profiles were measured using a 2-dimensional intensified camera placed a distance of 60 cm after the exit window of the amplifier cell. The Beamcode software used provided automatic Gaussian fits and beam waist sizes of the beam profiles.

3. RESULTS

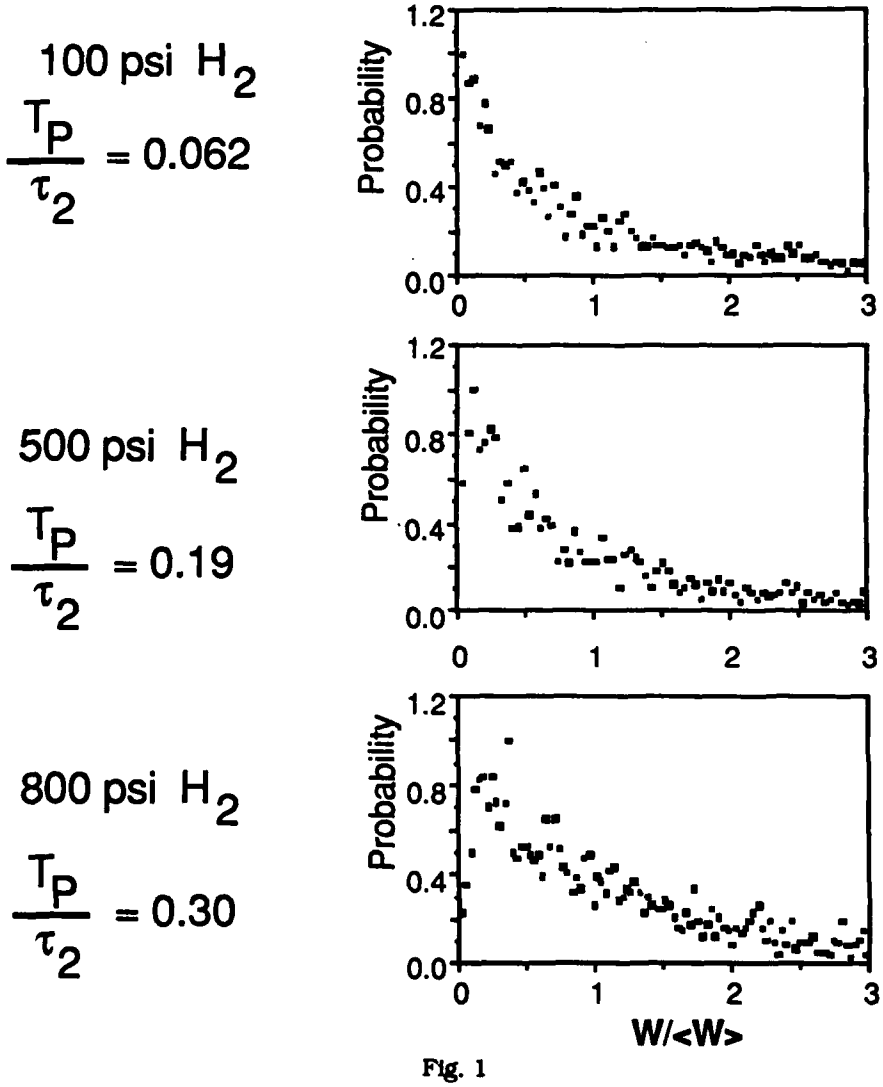

Fig. 1

In order to characterise our experiment, we initially looked at the statistics of the Stokes pulses using the amplifier cell as a self-generator, operated just above threshold. For a Fresnel number of 0.83, we were able to see the effects on the energy probability distribution function due to increasing the number of temporal modes by decreasing the degree of transiency. Results are shown in Fig. 1 for three different pressures of H_2 (7atm., T_P/τ_2 = 0.062; 34atm., T_P/τ_2 = 0.19; 55atm., T_P/τ_2 = 0.30) where T_P is the laser pulse duration and τ_2 is the dephasing time. The deviation from a negative exponential is seen in the lowest energy bins and the results follow closely that of other researchers.

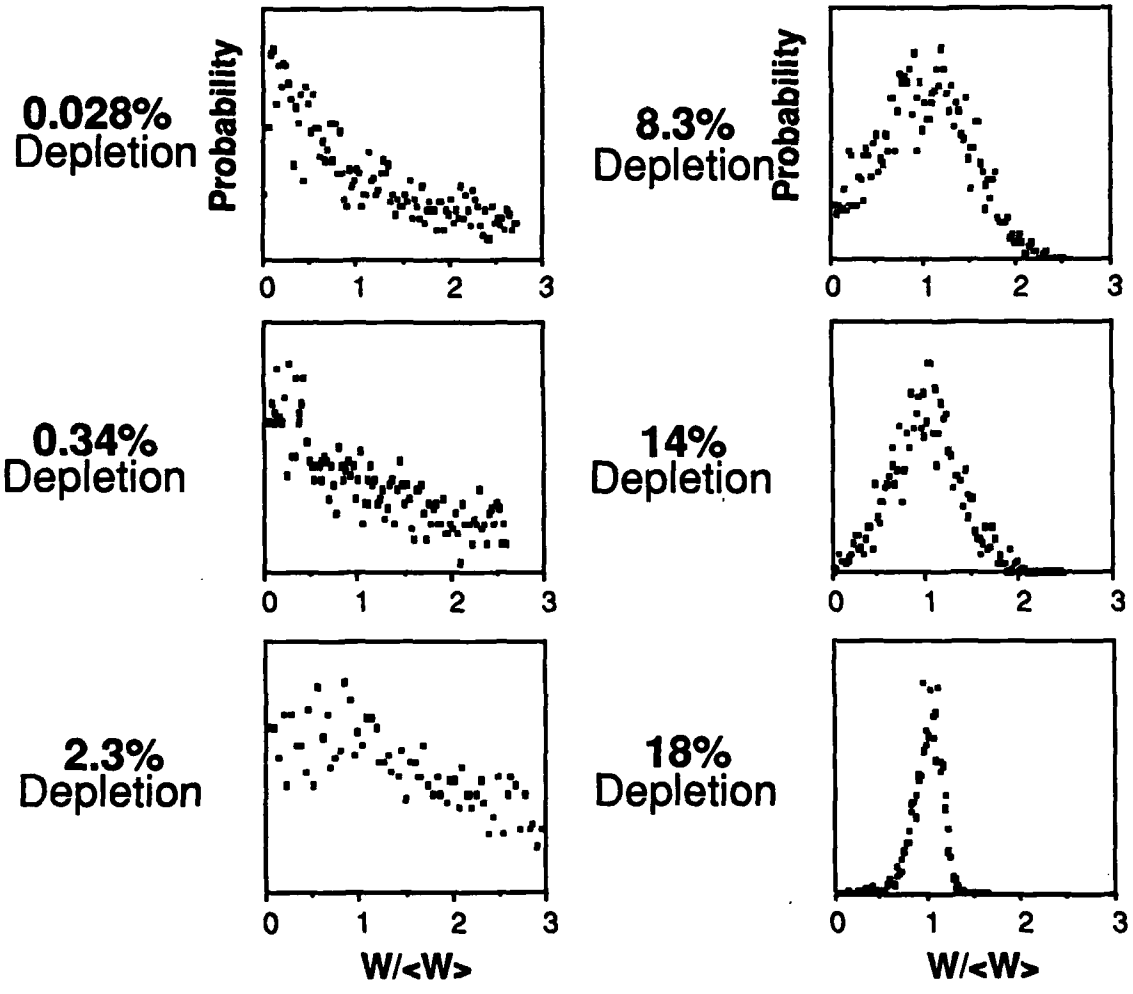

Fig. 2

The probability distributions of the self-generated Stokes is also shown as the transition from the linear to the nonlinear regime is made. The data in Fig. 2 were obtained with F = 0.83 and T_P/τ_2 = 0.062 as the pump energy was increased. For small depletion levels

a negative exponential distribution is reproduced. At 2.3% depletion a transition occurs and the distribution is essentially flat. With increasing depletion, a distribution with a well-defined peak centered at $W/\langle W\rangle=1$ is seen to narrow up rapidly.These results are in excellent agreement with the predictions of Lewenstein.

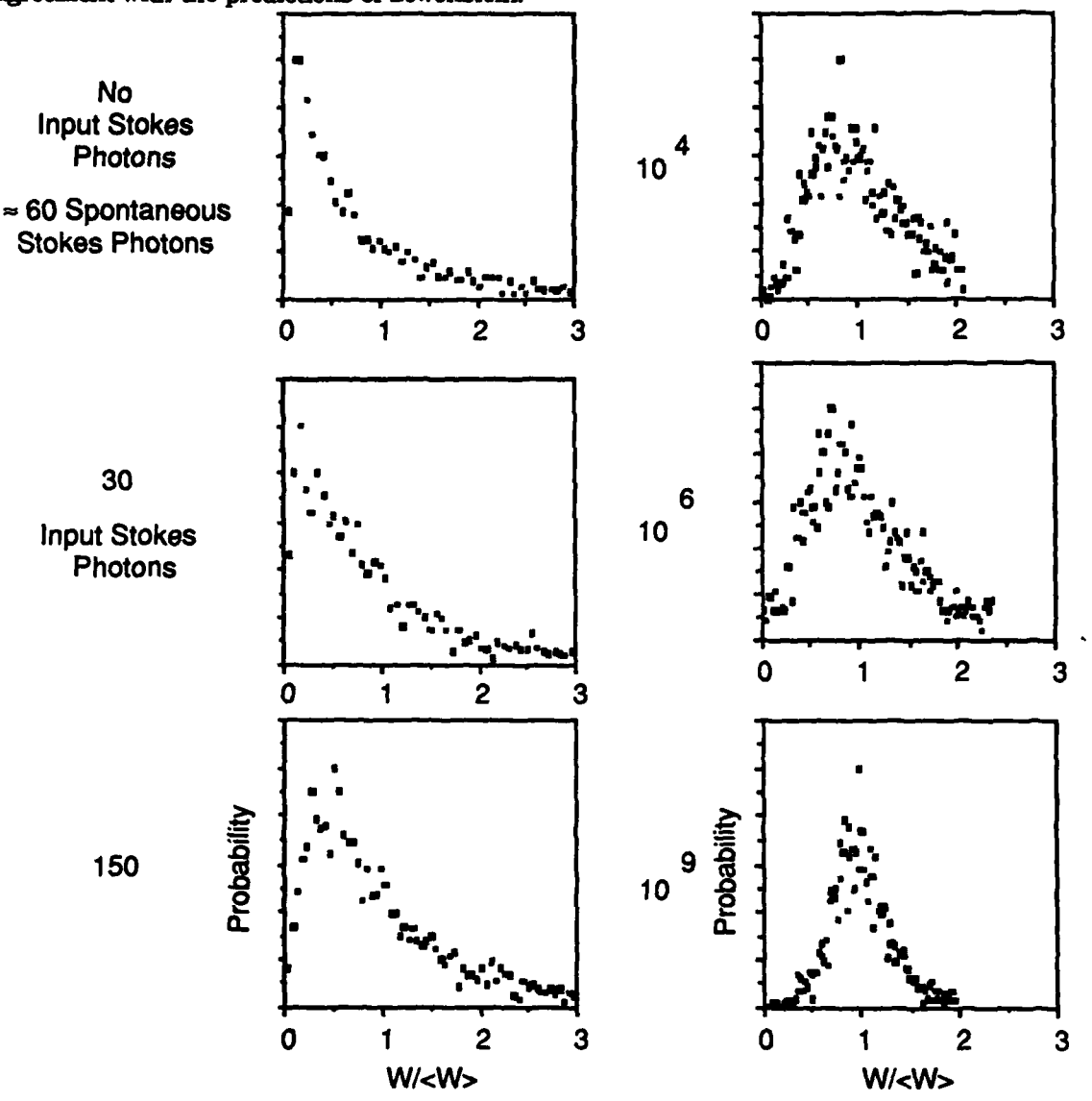

Fig. 3

The statistics of the amplified Stokes pulses were obtained with the same $F = 0.83$ and $T_P/\tau_2 = 0.062$ system and are shown in Fig. 3. In the absence of an input seed-Stokes pulse, the pump energy was just sufficient to drive the self-generator above threshold. Then, as the amount of seed Stokes was increased, the pump energy was decreased, to keep the amplified

Stokes at about the same level. Thus, one has amplification of a well-stabilized seed-Stokes distribution competing with self-generated Raman which builds from quantum noise in the amplifier itself.

It should be emphasized that the data used in Fig.3 were taken for a pump energy at, or below, visible threshold for Stokes production since, for higher pump energies the distribution quickly loses the negative exponential character. Using the computed average energies of the distributions we were able to estimate the ratio R, of chaotic to stabilized energy in the output Stokes pulses. The data aquisition system also calculated the average pump pulse energy for each data set and so the chaotic contribution could be scaled according to

$$\frac{W_2}{W_1} = \exp[2u(\sqrt{P_2} - \sqrt{P_1})] \times \sqrt{\frac{P_1}{P_2}}$$

where $W_{1,2}$ is the chaotic self-generated energy corresponding to the pump energy $P_{1,2}$ and $u=\sqrt{2}g_{ss}L/\tau_2 A$, with g_{ss} being the steady state gain.

In the narrow-band limit, the distribution of pulse energies due to a superposition of stabilized (W_{sta}) and chaotic (W_{ch}) energy components is given by

$$P(W)=\frac{1}{<W_{ch}>}\exp\left\{-\frac{W+<W_{sta}>}{<W_{ch}>}\right\} I_0\left\{\frac{2[W<W_{sta}>]^{1/2}}{<W_{ch}>}\right\}$$

where I_0 is the modified Bessel function of order 0. We have calculated the distribution $P(W)$ for values of $R= <W_{ch}>/<W_{sta}>$ corresponding to those encountered in the experiment and the results are shown in Fig. 4.

The similarities of Figs. 3 and 4 indicate that the amplified Stokes statistics are a reflection of the degree of stabilized to chaotic nature of the output. However, the actual ratio of the number of noise photons to the number of seed-Stokes photons is quite different. It is apparent that the presence of a large input seed-Stokes field significantly aids the growth of the noise photons via the phonon buildup established by the seed Stokes which precedes the pump-initiated noise photons. The noise-Stokes field and the seed-Stokes field interact in the nonlinear gain medium in such a way that the amplification of the minor field is enhanced.

The spatial profile of a near unity Fresnel number system is, of course, a near Gaussian. However, we do see the $1/e^2$ diameter of both the self-generated Stokes and of the non-saturated amplified Stokes beams as being significantly broader (2.3mm) than that of the input pump (1.5mm) or seed-Stokes (1.7mm) when measured at 60 cm after the amplifier cell exit window. This is presumeably due to gain narrowing followed by diffraction of the beam. When the output Stokes energy exceeds 30% of the pump energy, a strong halo reaching 25%

of the central intensity, becomes evident around a central component of diameter about 1.7mm.

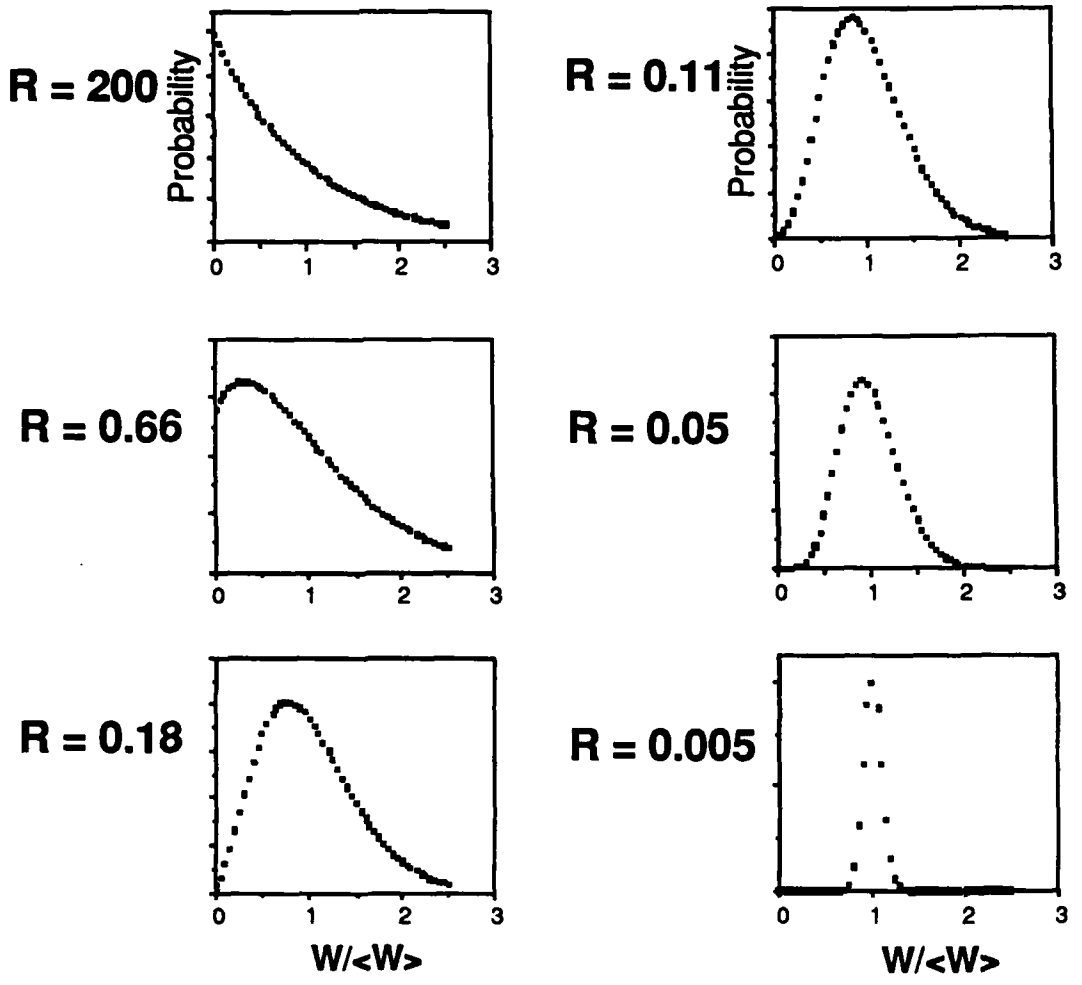

Fig. 4

With a Fresnel#5 pump system, the spatial profiles of the self-generated Stokes vary from shot-to-shot as shown in Fig. 5(a)-(c). However, for a F#10 input seed Stokes which overfills the pump volume, the amplified Stokes collapses down to a smoothe Gaussian with only a low level of input seed Stokes and the $1/e^2$ diameter (1.6mm) is smaller than that of either the pump (2.8mm) or the seed Stokes (4.2mm). The spatial mode of the amplified Stokes is shown in Fig. 5(d)-(f) for an input seed-Stokes pulse of 900 photons.

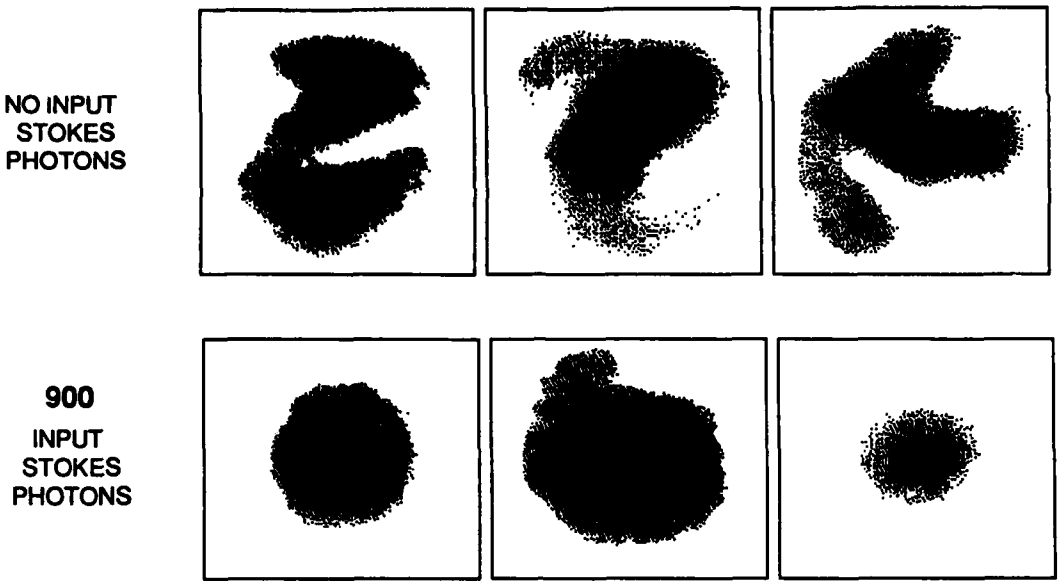

Fig. 5

For levels of about 100 input seed-Stokes photons the low energy shots show the random spatial distributions of intensity characteristic of the higher Fresnel number self-generated outputs, whereas the higher energy shots have a locked Gaussian nature. With injection levels of the order of 1000 seed-Stokes photons, the spatial mode has a locked character but the statistical distribution of Stokes energies is still dominated by a negative exponential character. There is an abrupt change in the statistics of the amplified Stokes energies for inputs between 10^3 and 10^4 photons when the negative exponential distribution changes over to a well-stabilized distribution centered about W=<W>. With increasing input seed Stokes, the spatial mode of the amplified Stokes remains Gaussian, developing a strong halo under saturation approaching 20% of the peak intensity of the central component.

Second Stokes Generation in Deuterium

ABSTRACT

We have investigated the growth, the spatial mode profiles and the pulse energy statistics of the first and second Stokes generated in a transient stimulated Raman self-generator experiment. In particular, we have observed two distinct regions of second Stokes growth. The first region is characterized by a low signal level due to 4-wave mixing. The second region appears to be one of stimulated growth seeded by spontaneous scattering at the second Stokes wavelength, an assumption supported by the rapid growth of the second Stokes signal and the observation of pulse energy statistics indicative of growth from noise. The absolute level of the Stokes signal in the 4-wave mixing region varied as a function of deuterium gas pressure, increasing for lower pressures as a result of stronger 4-wave mixing. We have also measured the second Stokes threshold as a function of deuterium pressure and have observed results consistent with first Stokes threshold measurements made at high pressures. At lower gas pressures, the threshold for second Stokes generation is lowered, indicating some seeding of the stimulated process due to 4-wave mixing.

EXPERIMENTAL APPARATUS

The general experimental apparatus used in these studies has been described above. In brief, a frequency-doubled Nd:YAG mode-locked laser with spatially filtered pulses of 40 ps duration and 5 mJ of energy at 532 nm was used to pump a Fresnel number one, single-pass Raman self-generator. The Raman cell was filled with deuterium at a pressure in the range of 45 to 145 atm. A separate seed-Stokes generator was operated well into saturation with a depletion level of about 15% to provide stable Stokes outputs at 633 nm and 780 nm for the purpose of calibrating photodiodes at these two wavelengths. The 532 nm pump beam had a confocal parameter well in excess of the 100 cm length amplifier cell used for these experiments. A two cell arrangement was used at certain times to clarify the role of first Stokes beam quality in the generation of the second Stokes. In those cases the first Stokes was generated in a separate cell and then spectrally isolated before being used to generate the second Stokes.

The input pump and the generated first and second Stokes pulse energies were measured with calibrated photodiodes. Gain and pulse energy statistics data were acquired automatically with a microcomputer-based data-acquisition system. Statistical data on the Stokes energy distributions were collected with 5% and 1% windows on the incident pump energy. Typical samples contained data from 2000 laser shots in the energy window with the data being collected into 100 energy bins of equal width. For gain measurements the natural

scatter of pump pulse energies was utilized in generating complete curves showing the dependences of the 1st and 2nd Stokes energies on pump energy. Spatial profiles of the pump, the 1st Stokes, and the 2nd Stokes were measured using a digital camera placed 35 cm after the exit window of the self-generator cell.

RESULTS AND DISCUSSION

The growth of the first and second Stokes in a single cell as a function of the 532 nm pump energy for two different deuterium pressures is shown in Fig. 1. The first Stokes follows the expected form of exponential growth followed by saturation. The second Stokes, however, has two separate growth regions, most clearly seen at high pressure in Fig. 1(a). The first is a 4-wave mixing region which is followed by a region of exponential growth. As seen in Fig. 1, the 4-wave mixing contribution is greater at lower pressures. At higher pressures, the phase-matching angle is greater and falls farther outside the angular spread of the pump and Stokes beams, reducing the strength of the 4-wave mixing process. At the lower pressure the 4-wave mixing region is not as distinct a region and seems to blend somewhat with the eventual exponential growth that the second Stokes undergoes. Figure 2 shows pulse energy statistics of the second Stokes measured at various points on the second Stokes growth curve of Fig. 1(a). Figure 2(a) shows pulse energy statistics characteristic of pulses produced by a well-stabilized source.

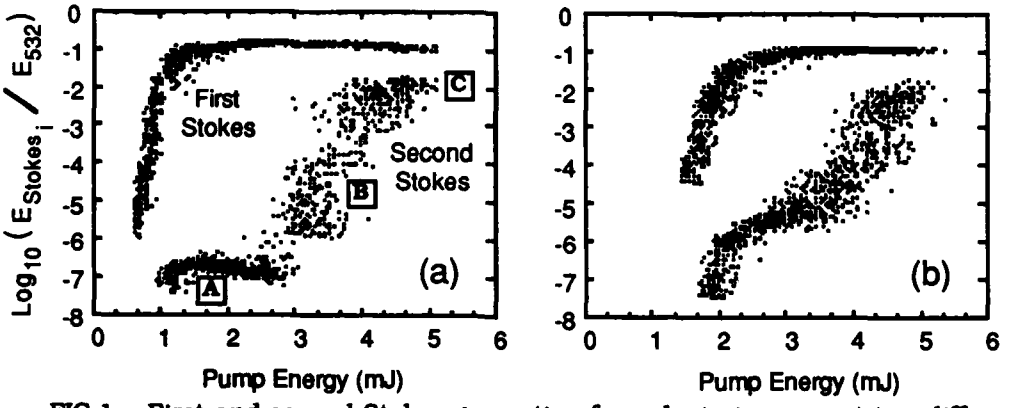

FIG 1. First and second Stokes generation from deuterium gas at two different pressures as a function of 532 nm pump energy. (a) Deuterium pressure of 1950 psi; (b) deuterium pressure of 700 psi. The boxed letters in figure (a) indicate regions where pulse energy statistics were measured (see Figure 2).

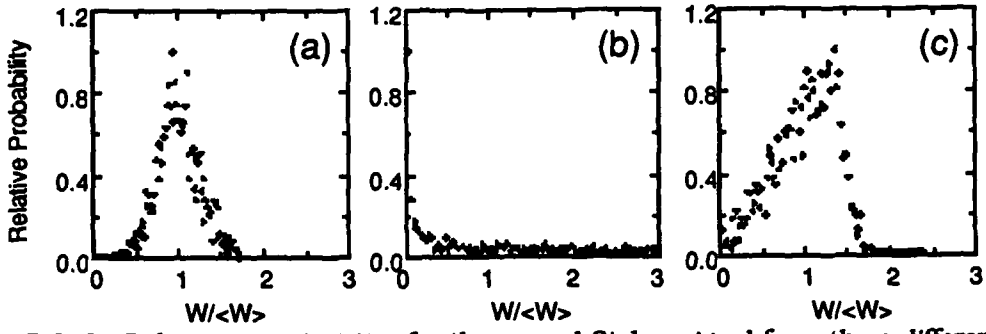

FIG. 2. Pulse energy statistics for the second Stokes signal from three different regions of Fig. 1(a): (a) from the 4-wave mixing region identified as **A**; (b) from the exponential growth region identified as **B**; (c) from the saturated region identified as **C**. W is the pulse energy and <W> is the average pulse energy.

This is consistent with production of the second Stokes signal by 4-wave mixing from a relatively constant energy pump and a saturated first Stokes. Figure 2(b) shows a pulse energy distribution measured in the exponential growth region for the second Stokes in Fig. 1(a). Here the distribution is highly peaked at a very low energy value, an indication that the pulses are generated from an extremely noisy source, such as quantum noise. However, the distribution is different than would be expected if the source was simply quantum noise. A further experiment performed with separate Raman cells for first Stokes and second Stokes generation showed that the excessively noisy nature of the distribution in Fig. 2(b) was caused by spatial beam degradation in the first Stokes light. When the degradation of the first Stokes beam quality was removed by spatial filtering, the distribution returned to a more normal negative exponential distribution typical of that produced by quantum noise. Figure 2(c) shows a pulse energy distribution taken from the region in Fig 1a where the second Stokes is beginning to saturate. The form of the distribution is consistent with a saturated process.

We have made threshold measurements for both first and second Stokes generation. We define threshold to be when the Stokes order of interest has reached an energy level that is 0.1% of that Stokes' pump energy. At high pressures we found that the threshold for second Stokes generation matched the first Stokes generation threshold very well. The values were obtained in a single cell and were corrected for effects such as reduced cell length for second Stokes generation and slightly reduced beam quality of the generated first Stokes. Other experiments have reported anomalously high thresholds for second Stokes generation. Explanations proposed have concentrated on the gain narrowing of the first Stokes beam and the subsequent reduction of second Stokes generation due to the diverging beam. Our experiments were performed using a collimated 532 nm pump beam to minimize any divergence problems. Detailed measurements indicate that the first Stokes does pick up

some excess divergence even though we saw no large effects of this divergence on the second Stokes threshold. At lower deuterium pressures the threshold for second Stokes is well below the first Stokes threshold. This is consistent with our observation of an increase in 4-wave mixing at lower pressures.

Unanswered questions remain concerning the generation of second Stokes light. At high pressures, why doesn't the second Stokes light generated from 4-wave mixing seed the stimulated gain and dominate the apparent growth from spontaneous scattering? Further work is in progress on evaluating the first and second Stokes growth in the transient limit, with quantum noise initiation correctly modelled and four-wave mixing included..

Parametric Raman gain suppression in D_2 and H_2

It has been known for many years that at exact phase matching Stokes/anti-Stokes coupling suppresses the normal exponential gain in stimulated Raman scattering. Bloembergen and Shen[1-3] showed that the stimulated Raman radiation would grow as a mixed mode containing both Stokes and anti-Stokes components. When the Stokes/anti Stokes interaction is not phase matched both waves grow exponentially, with the ratio of their intensities depending on the magnitude of the wave vector mismatch. Under phase matched conditions, however, the parametric coupling of the waves suppresses the buildup of the phonon population in the medium, terminating the growth of both optical waves. Such behavior has also been predicted in numerical solutions of the stimulated Raman equations[4].

Experimental evidence of gain suppression has been obtained primarily in self-generation experiments, in which it has taken the form of unexpectedly high thresholds, of dark regions in the Stokes emission[5-7] or of anti-Stokes emission at angles offset from the phase matching direction[8]. Additionally, Bloembergen[9] has reported Stokes amplification at levels below theoretical expectations. These experimental observations confirm a reduction of gain at phase matching, but they do not establish either the extent of the gain reduction or that the growth of the scattered radiation is non-exponential for the phase matched interaction.

Gain suppression because of Stokes/anti-Stokes coupling has been discussed theoretically in the literature only for steady-state interactions. We summarize the predictions of that theory below to indicate the source of gain suppression and some of its properties in the steady state. Although quantitative comparison of these predictions with the transient experiments described later in the paper is open to question, the fact that the experimental results reproduce the qualitative features of the steady state theory indicates that the same underlying physical principle applies to both regimes.

In the presence of Stokes/anti-Stokes coupling stimulated Raman scattering is described by the equations

$$dA_{AS}/dz = -K_1 |A_L|^2 A_{AS} - K_2 A_L^2 A_S^* \exp(-i\Delta kz) \quad (1a)$$

$$dA_S^*/dz = K_3 |A_L|^2 A_S^* + K_2(\omega_S n_{AS}/\omega_{AS} n_S) A_L^{*2} A_{AS} \exp(i\Delta kz) \quad (1b)$$

where $K_1 = -iK_{AS}\chi_{AS}$, $K_2 = -iK_{AS}(\chi_{AS}\chi_S^*)^{1/2}$, $K_3 = -iK_S\chi_S^*$. χ_S and χ_{AS} are nonlinear susceptibilities for stimulated growth of the Stokes and anti-Stokes waves, respectively, $K_{S(AS)} = 2\pi N\omega_{S(AS)}/n_{S(AS)}c$, N is the number density, and $\Delta k = k_S + k_{AS} - 2k_L$ is the wave vector mismatch.

For non-zero values of Δk the Stokes and anti-Stokes field amplitudes have exponential growth of the form exp(gz), with the gain coefficient g given by [2,3]

$$g = \mathrm{Re}\{(1/2)(K_3 - K_1)|A_L|^2 - (i/2)[\Delta k^2 + 2i\Delta k(K_3 + K_1)|A_L|^2 - (K_1 - K_3)^2|A_L|^4]^{1/2}\}. \quad (2)$$

When $\Delta k = 0$ the exponential gain in equation (2) goes to zero. Under this condition the Stokes and anti-Stokes waves grow non-exponentially, with amplitudes given by

$$A_S(z) = A_S(0)\{K_1/(K_1-K_3) - [K_3/(K_1-K_3)]\exp[-(K_1-K_3)|A_L|^2 z]\} + (\omega_S n_{AS}/\omega_{AS} n_S)[K_2/(K_1-K_3)]A_{AS}(0)\{1 - \exp[-(K_1-K_3)|A_L|^2 z]\} \quad (3a)$$

$$A_{AS}(z) = A_{AS}(0)\{[K_1/(K_1-K_3)]\exp[-(K_1-K_3)|A_L|^2 z] - [K_3/(K_1-K_3)]\} - [K_2/(K_1-K_3)]A_S(0)\{1 - \exp[-(K_1-K_3)|A_L|^2 z]\}. \quad (3b)$$

The growth of the Stokes and anti- Stokes amplitudes at phase matching is initially linear in z. It slows down as z increases until the condition $A_S(z) = -(K_1/K_2)\,A_{AS}(z)$ is asymptotically approached at large z, in which limit neither the Stokes nor the anti-Stokes wave grows further. The small-z limit of this solution has been given in reference 3, and the initial growth and eventual limitation of both waves has been described in numerical solutions in reference 4.

We have made measurements of stimulated Raman scattering in both H_2 and D_2. The pump radiation was a 30 picosecond pulse from a frequency-doubled, mode-locked, Nd:YAG laser . Typically, 1 mJ of the 532 nm radiation was used to drive a single-pass Raman seed generator and the remaining pump energy, up to 3 mJ, was used to pump the 1 m long Raman amplifier cell.

The seed Stokes and the amplifier pump beams were spatially filtered, their diameters were matched at the amplifier entrance with telescopes and the pulses were overlapped in time for maximum gain[10]. Both beams were used for the seeded amplifier measurements, while the Stokes seed beam was blocked for the self-generation experiments.

Fig. 1. Photograph of the far-field of a typical self-generated anti-Stokes emission pattern for H_2 at a pressure of about 14 atm.The dark band separating the two bright rings occurs at exact phase matching.

The far-field of a typical anti-Stokes emission pattern obtained from the single-pass generator at a H_2 pressure of about 14 atm using a collimated 0.5 mm diameter pump is shown in Fig. 1. The bright spot in the center arises from the phase mismatched anti-Stokes growth that accompanies the forward Stokes emission and effectively overlaps the far-field of the

pump. In the vicinity of the phase matching angle the anti-Stokes intensity increases rapidly as Δk decreases, forming the bright inner ring, and then drops precipitously at exact phase matching, forming the dark band between the bright rings. For angles larger than the phase matching angle, the anti-Stokes emission rises once again as Δk increases, but eventually decreases due to the reduced interaction length at larger angles , forming the bright outer anti-Stokes ring.

The angular diameter of the dark band, as measured with a silicon diode array at the focus of a 1 m lens, was independent of the pump intensity and varied as the square root of the pressure. At about 18 atm its measured diameter was 8.5 mrad ± 10%, in reasonably good agreement with the value of 7.4 mrad predicted for phase matching from published dispersion data[11]. The diameters of the bright anti-Stokes emission rings were dependent on pump intensity, with their angular offset from phase matching increasing with pump intensity. At a constant pump intensity the angular offset of the anti-Stokes emission rings from the phase matching direction varied as the square root of the gas pressure in agreement with the predictions of the steady state theory.[1] The fact that the diameter of the dark band was independent of pump intensity, coupled with the reasonably good agreement between the experimental angular radius of the dark band and the theoretical phase matching angle, indicates that it is the dark band, and not the bright emission bands, that satisfies the phase matching condition.This is to our knowledge the first experimental identification of the dark band in the anti-Stokes emission that was predicted by Bloembergen[1], although similar dark bands may be evident in the anti-Stokes rings reported by Maker and Terhune.[12]

The relative intensities of the bright emission rings, and hence the appearance of the anti-Stokes emission pattern, depended on the gas pressure. The two bright rings were prominent simultaneously only in the pressure range between about 12.5 atm and 35 atm. At pressures higher than this range the outer ring dominated the pattern, while at lower pressures only the inner ring was visible.

The Stokes radiation is emitted in a broad central angular cone with a dark band at the Stokes phase matching angle.[5] The large Stokes phase matching angles in H_2 made it difficult to obtain quantitative data in the region beyond the phase matching angle. Consequently, we chose to study the dependence of the Stokes gain on the crossing angle in D_2, in which the phase matching angle is smaller because of the smaller Rāman shift. For gain measurements in D_2 the probe and pump beams were focused in the center of the Raman amplifier. For the range of crossing angles used the two beams overlapped for approximately 2.6 cm, a distance short compared to the confocal parameter of 10 cm, allowing the gain to be measured in effectively the plane wave limit.

The far field of a typical self-generated Stokes emission pattern produced in D_2 at about 20 atm is shown in Figure 2. It consists of a large, diffuse emission region in the center, a dark band, and emission at larger angles. The small bright spot within the dark band is our Stokes probe beam. The dark band corresponds to the region of non-exponential gain around the Stokes phase matching angle. At larger angles the Stokes gain again increases, but, because of the reduced interaction length, emission in this region is visible only where it was seeded with the Stokes probe beam . This pattern is similar to ones reported previously by several authors [5,7,13].

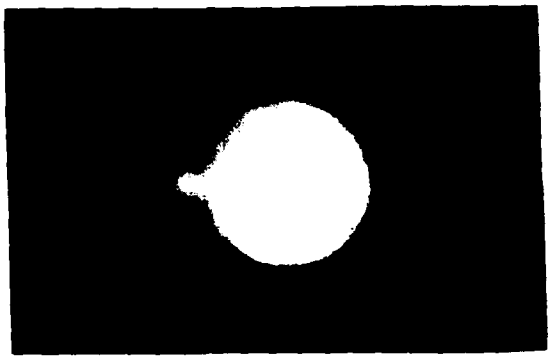

Fig. 2. Photograph of the far-field of a typical self-generated Stokes emission pattern for D_2 at a pressure of about 20 atm. The central cone and part of the outer band is clearly seen. The bright spot within the dark band is the seed Stokes beam.

Measurements of the amplification of the Stokes seed in D_2 at 41 atm as a function of pump energy at pump- probe crossing angles of 5, 7, and 9 mrad are shown in Figures 3a, b and c, respectively. The curve in Fig. 3a was obtained at an angle slightly smaller than the phase matching angle, corresponding to the edge of the central emission region in Fig. 2; the curve in Fig. 3b was obtained at the phase matching angle; and the curve in Fig. 3c was obtained at an angle greater than the phase matching angle, corresponding to the center of the outer arc of the pattern in Fig. 2. These measurements show exponential growth for the Stokes wave at angles on either side of the phase matching angle. Amplifications up to approximately 10^7 were obtained off phase matching, with pump depletion limiting the gain at the high end. The extrapolated amplification at the highest pump energy in the absence of depletion would have been 10^9. [10] For a given laser intensity , the gain was higher for the smaller angle (Fig. 3a) because of the longer interaction length. In contrast, the maximum amplification at the phase matching angle was approximately a factor of two for the highest pump energy and the growth is evidently not exponential in nature, demonstrating a suppression of Stokes amplification by at least a factor of 10^7. Positions of equivalent gain-length products are indicated by the vertical lines in the figures.

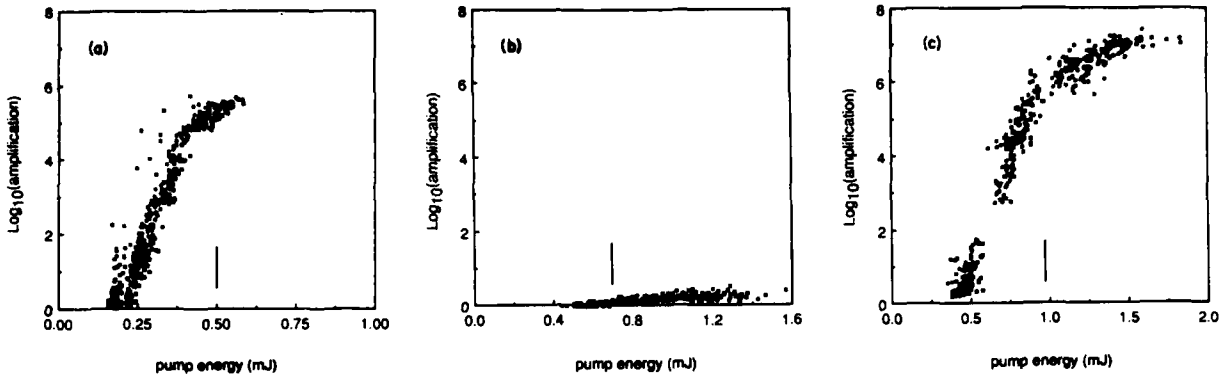

Fig. 3. Amplification of a Stokes seed pulse in D_2 at 41 atm as a function of pump energy at three different crossing angles. (a). A crossing angle of 5 mrad, corresponding to the outer edge of the central emission pattern in Fig. 2; (b) Exact phase matching at 7 mrad; (c) A crossing angle of 9 mrad, corresponding to the center of the outer arc in Fig. 2. The vertical lines in each picture indicate positions of equivalent gain-length product.

In summary, the results presented here are the first quantitative measurements of parametric gain suppression in stimulated Raman scattering. They show that the amplification of the Stokes wave at phase matching is lower than that on either side of the phase matched angle by at least seven orders of magnitude, and they confirm predictions that the growth of the Stokes wave under phase matched conditions is not exponential. While the general features of gain suppression in the transient regime covered by our experiments are apparently governed by the same underlying physical principle as those of the steady state theory, some of the quantitative details, such as the angular extent of the gain-suppressed region, could be affected by the transient response.

References

1. N. Bloembergen, Non-Linear Optics, Benjamin Press, N. Y. (1965).
2. N. Bloembergen and Y.R. Shen, Phys. Rev. Letters, 12, 504 (1964).
3. Y. R. Shen and N. Bloembergen, Phys. Rev. 137, A1787 (1965).
4. A. P. Hickman, J. A. Paisner and W. K. Bischel, Phys. Rev. A, 33, 1788 (1986).
5. R. Chiao and B.P. Stoicheff, Phys. Rev. Lett. 12, 290 (1964).
6. B.N. Perry, P. Rabinowitz and O.S. Bomse, Opt. Lett. 10, 146 (1985).
7. G. V. Venkin, G. M. Mikheev, and O. A. Novodvorskii, Kvant. Elekt. (Moscow) 12, 2230 (1985).
8. R. W. Hellwarth, F. J. McClung, W. G. Wagner and D. Weiner, Bull. Am. Phys. Soc.9, 490 (1964).
9. N. Bloembergen, Am. J. Phys. 35, 989 (1967).
10. M. D. Duncan, R. Mahon, J. Reintjes and L. L. Tankersley, JOSA B,5,37 (1988)
11. International Critical Tables, vol. 7, McGraw-Hill, NY. (1930)
12. P. D. Maker and R. W. Terhune, Phys. Rev. 137, A801 (1965).
13. For a review see A. N. Arbatskaya, in Proceed. of P. N. Lebedev Inst., vol. 99, N. G. Basov, ed. (1977), p. 1.[American Translation 1982]

Wavefront Studies in a Transient Raman Amplifier

PROBLEM: **IDENTIFY THE EFFECTS OF TRANSIENT RAMAN AMPLIFICATION ON THE INPUT STOKES WAVEFRONT.**

PARTICULARS: High quality pump with either high quality or aberrated Stokes wave.

VARIABLES:

High quality Stokes	Aberrated Stokes
• Timing between Stokes and Pump	• Timing between Stokes and Pump
• Level of gain	• Level of gain
• Degree of saturation	• Degree of saturation
	• Depth and spatial frequency of aberration

POSSIBLE EFFECTS:

Gain narrowing →  Input  Output (Different from steady state -- different intensity dependence)

Phase pulling → Pump and Stokes are phase modulated
Optimal gain at non-coincident timing
Stokes phase is pulled into correlation w/pump

Techniques to Evaluate Beam Quality

FOR HIGH QUALITY BEAMS:

- *Power in the bucket*
- Near field/far field measurements
  ---- compared with -----
  Far field calculated from near field data

FOR ABERRATED BEAMS:

- Observe the distortion of interferometer fringe patterns

Experimental Apparatus

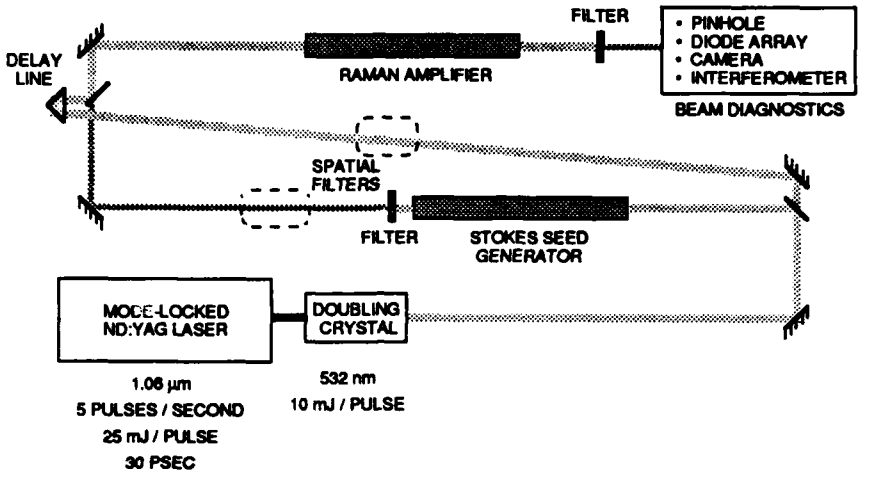

Power in the Bucket Measurements

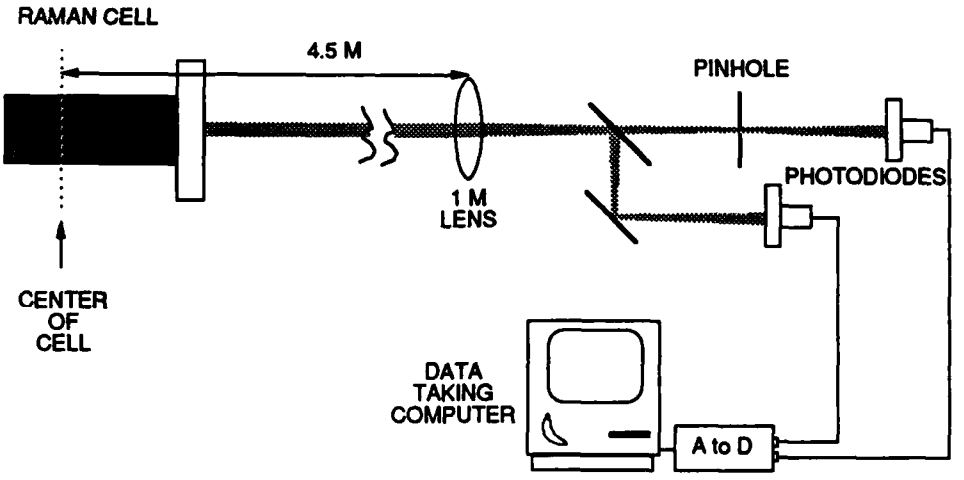

Power in the Bucket Results

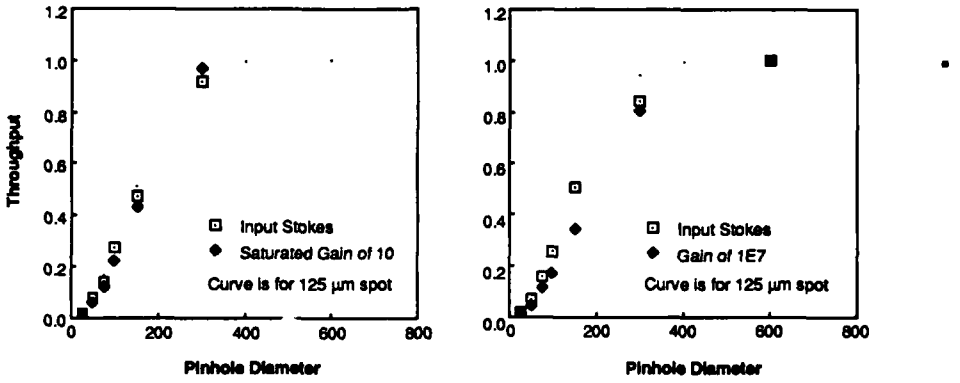

Near Field / Far Field Imaging

1. DIVERGENCE NOT TAKEN OUT

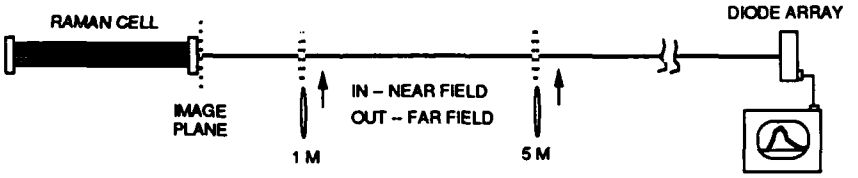

2. DIVERGENCE TAKEN OUT

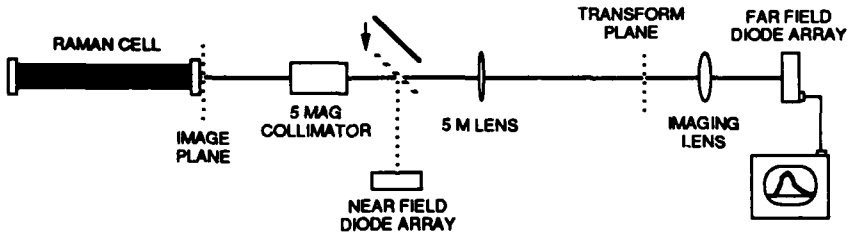

GAIN NARROWING IN THE NEAR FIELD

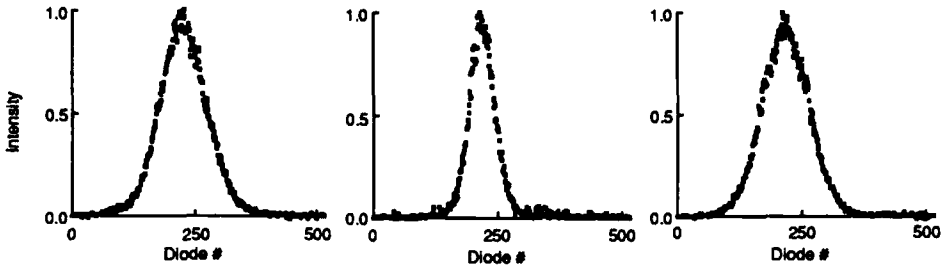

Input Stokes | High Gain Unsaturated | Saturated Gain

FITTING PROCEDURE

Near Field Data

Smoothed Normalized Chopped

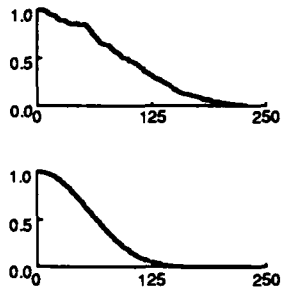

Fourier Transform using Experimental Constants

Far Field Data

Gaussian Fit

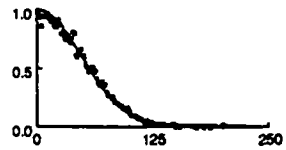

Final Comparison

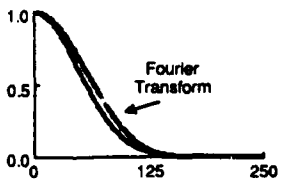

INPUT STOKES FITS

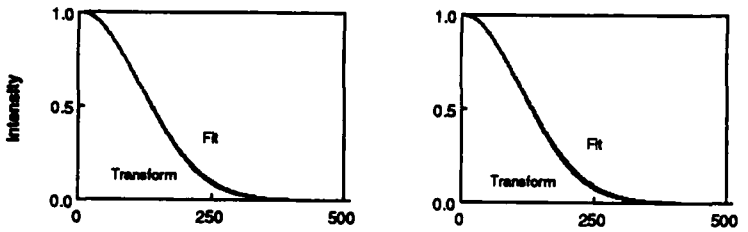

INPUT PUMP FITS

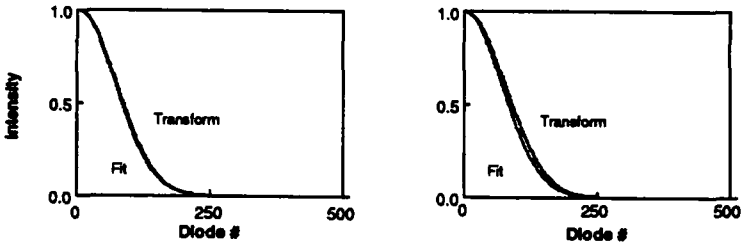

FITS WITHOUT DIVERGENCE REMOVED

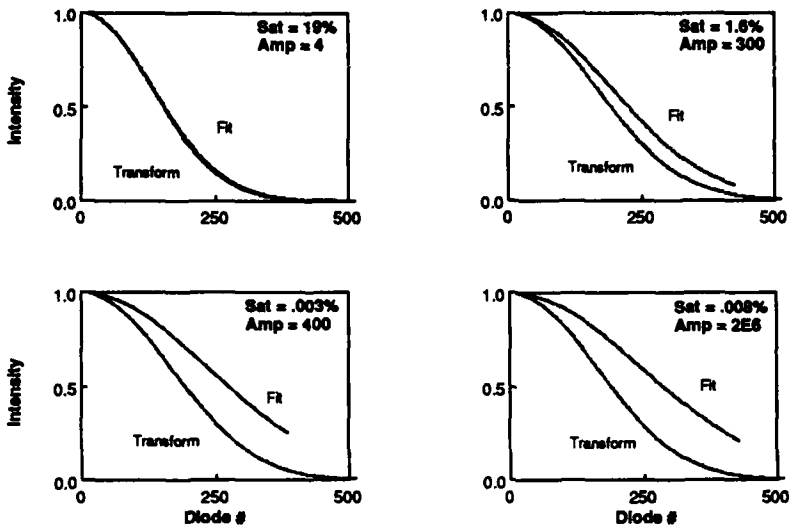

FITS WITH DIVERGENCE REMOVED

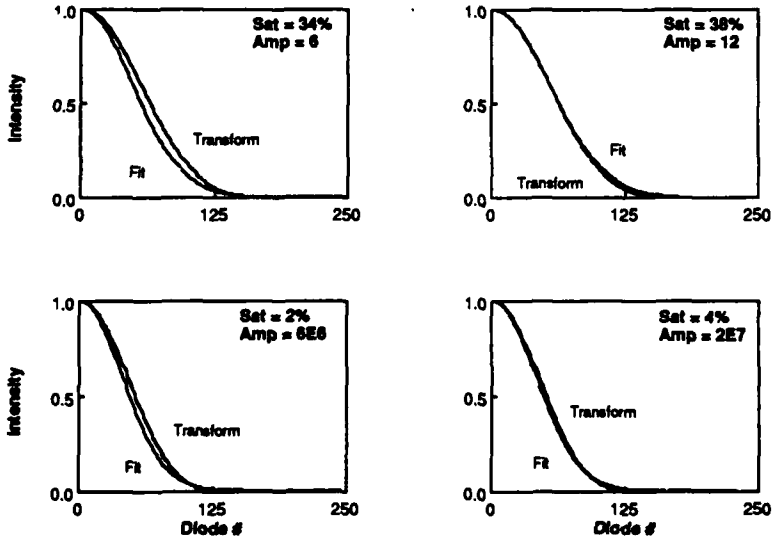

ABERRATED STOKES INPUT

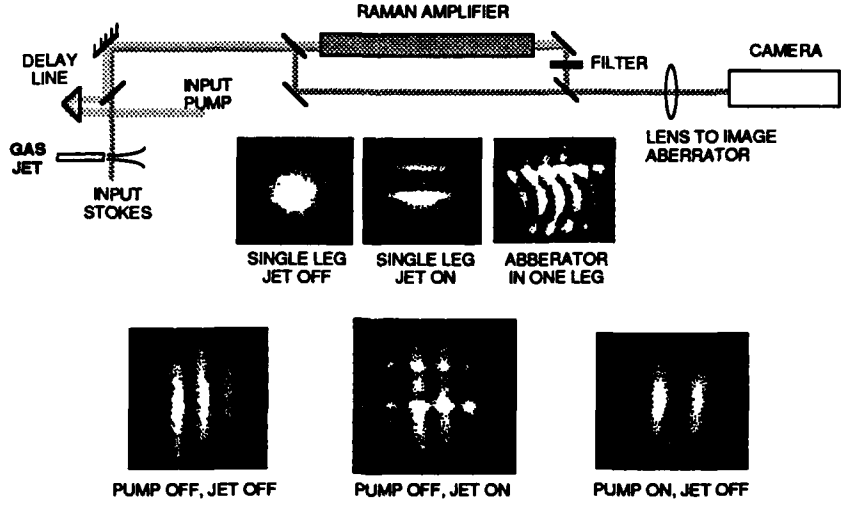

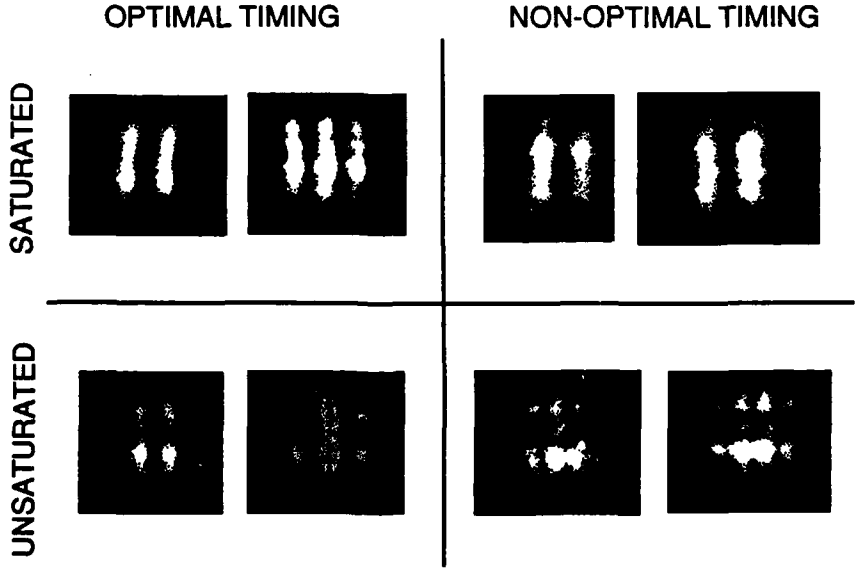

CONCLUSIONS

HIGH QUALITY STOKES INPUT

- Inherent quality of the Stokes beam is preserved under transient Raman amplification.
- Under high gain, unsaturated conditions, gain narrowing occurs. This introduces uniform spherical curvature that can be removed.

ABERRATED STOKES INPUT

- Aberrations with low spatial frequency and depth < 1 wave are preserved.
- Aberrations preserved for saturated and unsaturated amplification.

Transient Raman Amplification in a Crossed Beam Geometry

We describe results of experiments in a crossed-beam transient Raman amplifier that examine spatial quality of the amplified Stokes beam, beam combining properties, and effects related to replication of the crossing pump beams. The experimental measurements were made using 40 ps pulses produced by a mode locked Nd:YAG laser doubled to 532 nm. The seed Stokes at 683 nm was produced in a self-generator cell filled with hydrogen gas at 25 atm. Both the seed Stokes and the pump beam were spatially filtered before being combined with a variable delay and collimated to have confocal parameters in excess of the 1 m length of the amplifier cell. The pump was split into two beams and crossed in the center of the amplifier cell. An intensified camera was used to record the near-field spatial profiles of the amplified Stokes. This data was then Fourier transformed and compared with measured far field profiles to give an indication of beam quality of the amplified Stokes.

Motivations for the Present Work

- Investigate Level of Transient Amplification Using Two Pump Beams
- Investigate Conversion Efficiency
- Determine Beam Quality of Amplified Stokes

Experimental Apparatus

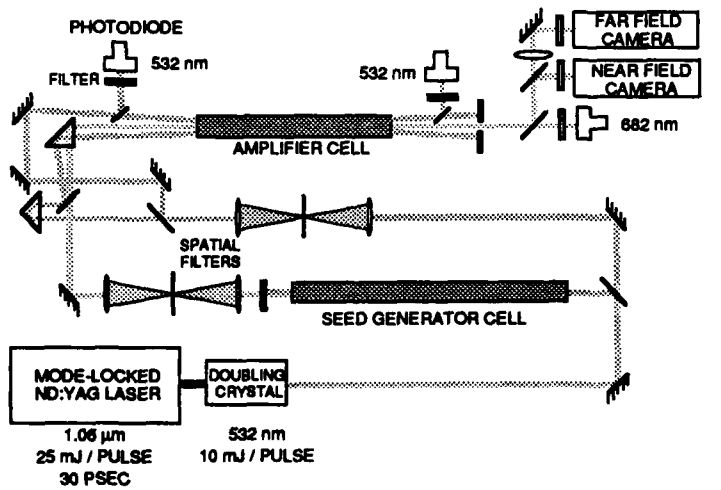

Near Field / Far Field Images

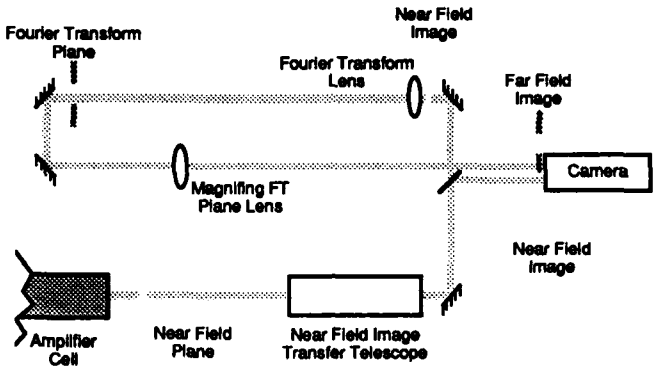

Amplification vs. Energy

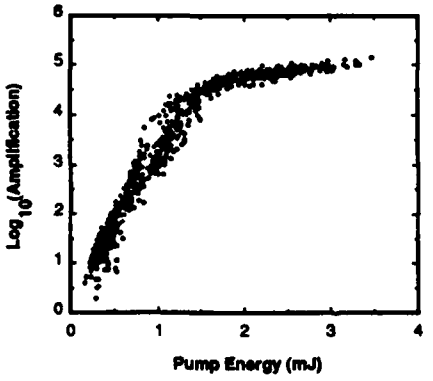

H_2 at 400 PSI

Crossed Beam Geometry:
4 mrad 1/2 angle

Collimated Beams

30 cm Effective Gain Length

Beam Quality Analysis

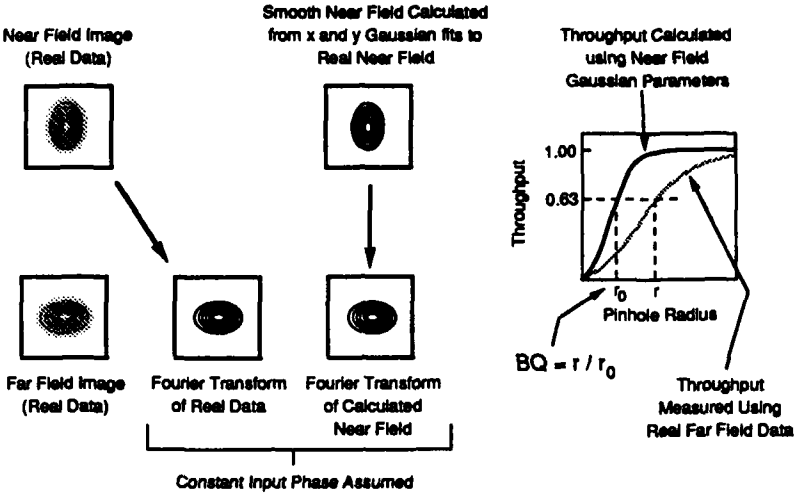

Seed Stokes Beam Quality

NRL

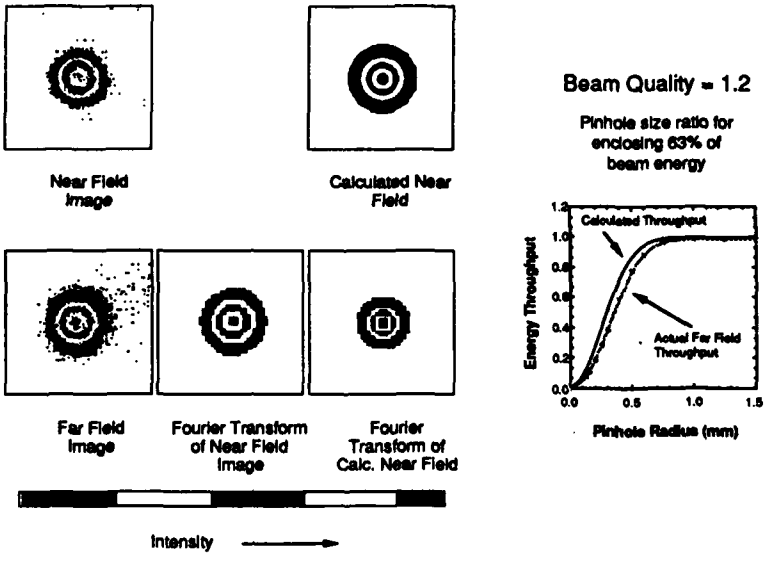

Amplified Stokes Beam Quality

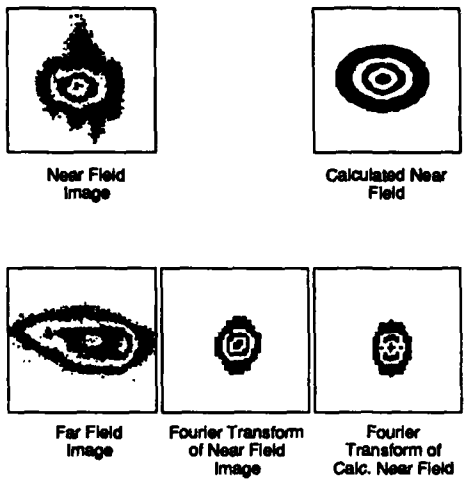

Beam Quality = 2.4

High Gain
Pump/Stokes = 50
37 % Energy Conv.

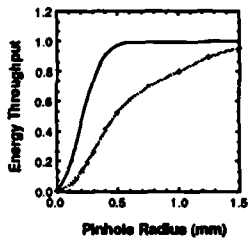

Amplified Stokes Beam Quality

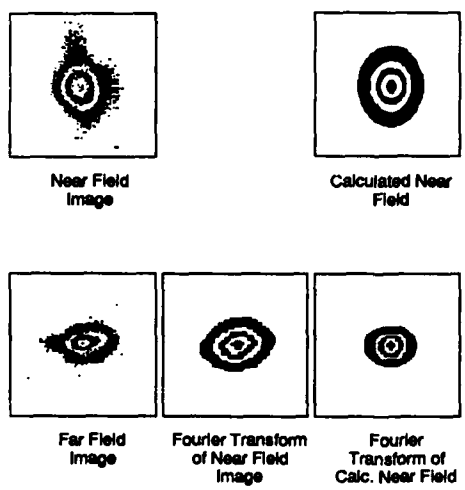

Beam Quality = 1.05

Moderate Gain
Pump/Stokes = 5×10^3
12 % Energy Conv.

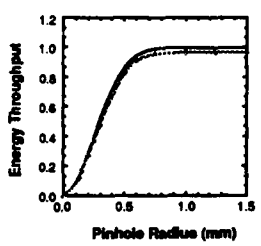

Amplified Stokes Beam Quality

Near Field Image

Calculated Near Field

Far Field Image

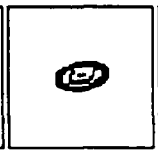

Fourier Transform of Near Field Image

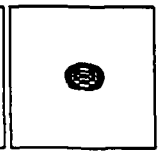

Fourier Transform of Calc. Near Field

Beam Quality = 1.3

High Gain
Pump/Stokes = 5×10^6
5 % Energy Conv.

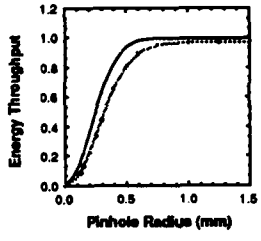

Amplified Stokes Beam Quality

Near Field Image

Calculated Near Field

Far Field Image

Fourier Transform of Near Field Image

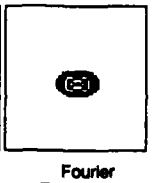

Fourier Transform of Calc. Near Field

Beam Quality = 1.8

Moderate Gain
Pump/Stokes = 10^6
0.1 % Energy Conv.

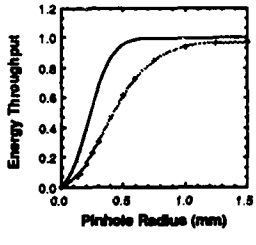

Summary

- Amplification Using 2 Pump Beams
  - Amplification is adequate to reach saturation
  - Saturation is softer than for single pump amplification
- Conversion Efficiency
  - Maximum photon conversion efficiency ≈ 40%
  - Less than for single pump
- Stokes Beam Quality
  - Highly saturated gain conditions degrade the Stokes substantially
  - No observed pump replication (4-wave mixing induced)
  - Low saturation, moderate gain gives best amplified beam quality
  - This is not the optimal geometry to use for dual beam energy transfer!

Narrow Linewidth Unstable Resonator

Unstable resonators are effective in producing low divergence, high power radiation from high gain lasers, such as excimer, dye, Nd:YAG and infrared molecular lasers. For many applications, narrow linewidth is required in addition to low divergence and high power. Narrow bandwidth operation of various unstable resonators has been described. [1-5] In one configuration, commonly used for single line operation of CO_2 and HF lasers in the infrared,[3-5] the frequency narrowing elements are added to a linear cavity as end reflectors or internal transmissive elements. However, the effectiveness of such configurations for producing narrow-bandwidth radiation is limited in principle because the light passing through the frequency-narrowing elements is highly diverging on at least one pass through the cavity. Broadening of the linewidth or restriction of the aperture over which narrow-bandwidth radiation is obtained can ultimately result. These limitations are more significant at shorter wavelengths because of the wavelength-scaling characteristics of the bandwidth and acceptance angle of common frequency narrowing elements.

Alternative configurations that have expanding telescopic optics and extensive collimated regions that potentially can be used for frequency-narrowing optics have been described.[1,6,7] One of these consists of a ring around the gain medium with one pass through the gain medium per roundtrip.[1,6] In the other, the beam makes two passes per roundtrip through the gain medium at a small angle, with a cavity length sufficient to separate the incoming and outgoing beams for outcoupling. Finally, Alexseev et al [8] have described a composite narrow-band system consisting of two cavities with a common mirror. One cavity is stable and provides narrow-band radiation. The outer edges of the mode pattern couple into the unstable resonator for amplification.

Because of the angular-acceptance limitations associated with unstable resonators, narrow-linewidth radiation is commonly produced in oscillator-amplifier systems using stable resonators. Low-power, low-divergence, narrow-linewidth radiation is generated in the stable resonator and is subsequently amplified to high power in one or more gain stages which can operate either as amplifiers or injection locked oscillators.

In this paper we describe the use of an asymmetric ring in the feedback section of a negative-branch unstable resonator to allow operation at arbitrarily narrow linewidths while simultaneously filling the entire laser aperture. This cavity eliminates the usual limitation on narrow-bandwidth operation of an unstable resonator by ensuring that only collimated light passes through or reflects from the frequency-narrowing optics. One advantage of the cavity is that the multiple stage laser systems that are usually used for the production of low-

divergence, narrow-bandwidth, high-power radiation can be replaced with a single laser. Size, cost, and complexity thus can be reduced while reliability is increased.

An unstable resonator with the asymmetric feedback ring was used. Collimated light propagating from right to left is outcoupled by a scraper. The light in the Fresnel core passes through a hole in the scraper and into the feedback ring through a beamsplitter with 50% reflectivity. In the ring the light passes through or reflects from any of several frequency narrowing optics such as gratings, etalons or prisms. Shown for purpose of example is a single etalon. The light is then focused by a lens, after which it diverges and reflects from the beamsplitter back into the main cavity. The light is recollimated by the output mirror and starts another cavity round trip. An aperture at the focus of the forward-travelling beam in the ring blocks most of the backward circulating beam, which has a relatively large diameter at that point. Feedback from the ring then occurs primarily from the forward-travelling beam that passes through the etalons while collimated.

In the experiments described below we have demonstrated the use of this cavity with a XeCl laser to produce single-line radiation with a linewidth of 0.15 cm^{-1}. We used a Lumonics model TE-861M-4 electric discharge laser with uniform discharge electrodes. The output mirror had a 3 m radius of curvature and the lens in the feedback ring had a focal length of 30 cm, providing a cavity magnification of 5. A scraper with a 3.5 mm hole then provided a maximum output beam diameter of 17.5 mm, which did not completely fill the 3 cm by 2 cm gain aperture. A 15mm aperture in front of the output mirror was used to mask the unused gain region.

Single-line selection and coarse frequency-narrowing were done with a 99 μm air-spaced, piezoelectrically-tuned etalon with a finesse of about 15. Operation on either of the two main gain lines at 308.0 nm or 308.2 nm could be selected by tuning the 99-μm etalon. Further frequency narrowing was accomplished with the addition of either a second air-spaced, piezoelectrically-tuned etalon with a spacing of 0.94 mm (finesse = 15) or a 5 mm solid quartz etalon (finesse = 11). The performance of the cavity was assessed qualitatively by recording the output beam profile (at a distance of 150 cm from the scraper) and the ring pattern obtained from an appropriate Fabry-Perot (FP) interferometer on photographic film , while simultaneously verifying single-line operation with a grating spectrometer. Quantitative determination of the linewidth was determined from diode array measurements of the FP rings. Pulse durations and output energies were measured with a photodiode and an energy meter.

The output beam profile and the ring pattern were obtained from an air-spaced FP interferometer with a free spectral range (FSR) of 5.3 cm^{-1} when the cavity was operated with only the 99 μm etalon adjusted to select the 308.2 nm line. The output profile was uniform

across the full 1.5 cm aperture allowed by the cavity optics, with a center hole corresponding to the hole in the scraper and some structure due to Fresnel diffraction from the edges of apertures in the cavity. The pattern obtained from the FP interferometer shows excellent ring definition.and diode array measurements gave a bandwidth of 1.2 cm^{-1}.

Further line-narrowing was accomplished by adding either the 0.94 mm air-spaced or the 5 mm solid etalon to the feedback ring. The output beam profile and the ring pattern were obtained from a FP interferometer with an FSR of 0.56 cm^{-1} using the 99 μm air-spaced and 5 mm solid etalons in the cavity. Again the output profile was uniform across the full aperture. The linewidth for this case was 0.15 cm^{-1}. Similar performance was obtained when the laser was tuned to the other main laser line at 308.0 nm, and when the 0.94 mm air-spaced etalon was used in the cavity in place of the 5 mm etalon.

In order to assess the effectiveness of our feedback ring in obtaining arbitrarily narrow-bandwidth radiation we have compared its performance to that of a linear, frequency-narrowed, negative-branch unstable resonator with the same magnification as the ring cavity. The linear cavity was operated using the 99 μm etalon either by itself or with the 5 mm solid etalon. When the 5 mm etalon was used it was placed between the lens and the rear mirror to minimize the angular divergence of the light that passed through it.

The output beam profile and the ring pattern from the 5.3 cm^{-1} FP interferometer obtained when only the 99 μm etalon was used in the linear cavity were measured. The output profile was again uniform over the full available aperture and the linewidth was 0.85 cm^{-1}. When the 5 mm solid etalon was added to the linear cavity, the output beam profile was again recorded. In this situation the output profile was confined to a small region of the available aperture, consisting essentially of an arc of the etalon transmission ring. This type of pattern resulted because the etalon had to be tilted sufficiently far from normal incidence to prevent lasing from its faces. The radiation contained within the restricted lasing region had a bandwidth of the order of 0.16 cm^{-1}. However, because of the angular acceptance properties of the cavity etalon, the narrow-bandwidth radiation could not be obtained over the full aperture. Indeed, careful analysis of the ring pattern shows a broad-band, low-intensity component indicative of the wider linewidths present across the full aperture.

We also compared the output energy and pulse duration of the radiation of the ring and a linear unstable resonator. Although the energy of the untuned Linear cavity is twice that of the untuned ring cavity, the energy obtained from the two cavities with one etalon is comparable, and the ring cavity provides 2.5 times the energy of the linear cavity with two etalons. Pulse duration also decreases for each cavity as etalons are added.

We also attempted to operate an unstable ring resonator of the type described in reference 6, but we were unable to raise it above threshold with the Lumonics laser. We attribute

this result to a combination of the long cavity length of this configuration, the limited gain duration of the Lumonics laser and the fact that the radiation passed through the gain medium only once per cavity round trip. The importance of the shortest possible cavity length is supported by our observation that if we stretched our ring cavity until it was comparable in length to the one just described, it also operated below threshold .

References

1. W. H. Steier, "Unstable Resonators", in Laser Handbook, vol. 3, M. L. Stitch, ed., North Holland, 1979, 1986.
2. Yu. A. Anan'ev, N. I. Grishmanova, I. M. Petrova and N. A. Sventsitskaya, Kvant. Elektron. (Moscow) **2**, 738 (1975) [Eng. Trans: Soviet J. Quant.Elect. **5**, 408 (1975)].
3. R. A. Chodzko, H. Mirels, F. S. Roehrs,, and R. J. Pedersen, IEEE J. Quant. Elect. **QE-9**, 523 (1973).
4. R. A. Chodzko, Appl. Opt. 13, 2321 (1974).
5. B. K. Deka, P. E. Dyer and I. K. Perera, Appl. Opt. **18**, 3722 (1979).
6. R. J. Freiberg, P. P. Chenausky and C. J. Buczek, IEEE J. Quant. Elect. **QE-10**, 279 (1974).
7. J. M. Bernard, R. A. Chodzko, and H. Mirels, Appl. Opt. **25**, 666 (1974)
8. V. A. Alekseev, V.G. Nikiforov, and A. V. Shulenin, Zh. Prik. Spek. **41**, 244 (1984) [English trans: J. Applied Spectroscopy **41**, 912 (1984)].

Stable/unstable coupled resonator

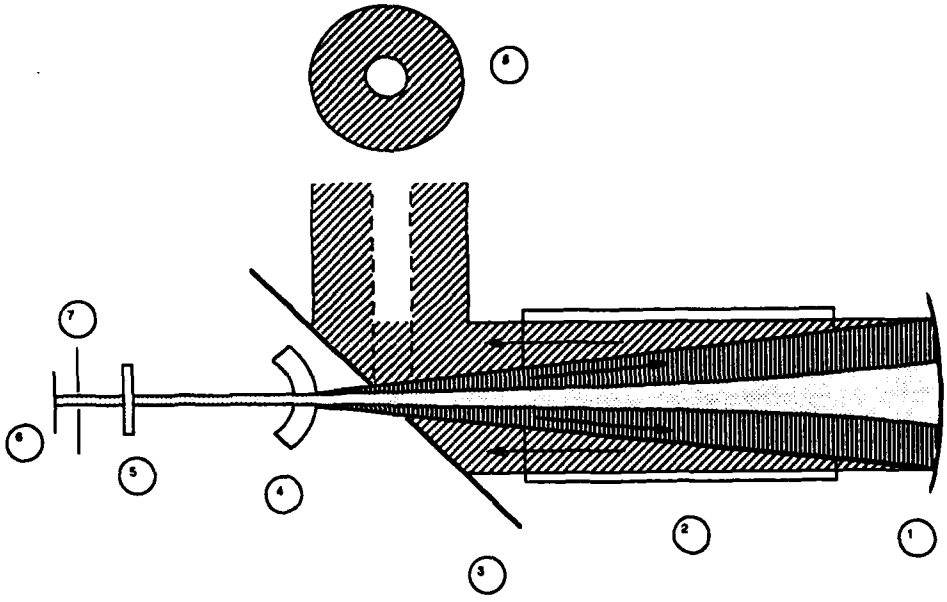

The coupled stable/unstable resonator offers the possibility of frequency-narrowing an unstable resonator without using a ring geometry. The curved output mirror and the convex surface of the intracavity optic form the unstable resonator cavity. The curved output mirror and the flat mirror form the restricted-aperture stable resonator. This arrangement is possible because the convex and concave surfaces of the intracavity optic have the same radius of curvature. The stable cavity is suitable for frequency-narrowing of the laser radiation, a portion of which is injected into the unstable cavity on each cavity round-trip. In the unstable cavity, the narrow-band radiation is expanded, amplified, and coupled out. Single-line operation has already been demonstrated using this hybrid cavity with XeCl in a commercial electric discharge laser.

Unstable resonator with output ring

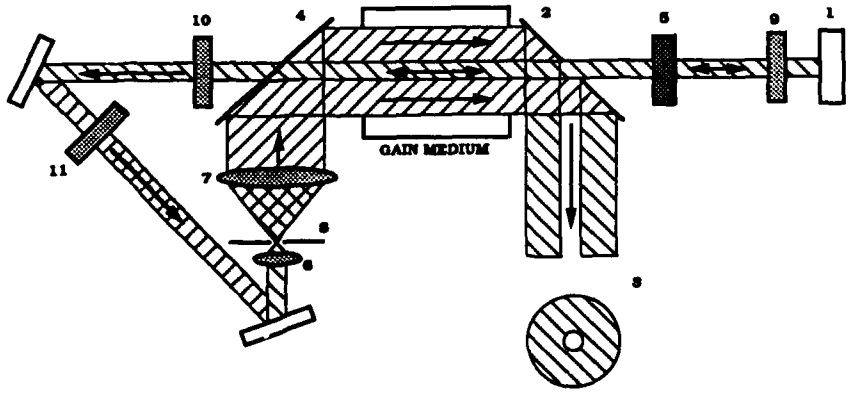

The unstable resonator with an output ring was conceived as an alternative to the unstable resonator with a feedback ring. The major advantage of the alternative cavity is the possibility of placing frequency-narrowing elements in a position in the cavity where highly collimated laser radiation passes the elements twice per cavity roundtrip. The potential for frequency-narrowing is thus much greater in the cavity with the output ring. Operation of the cavity with the output ring requires optical isolation for suppression of the reverse-travelling wave. An optical isolator for 308 nm radiation, based on the Faraday effect is under development. To date, a 6000 Gauss permanent magnet assembly has been designed, constructed, and characterized. Initial experiments on Faraday rotation of linearly polarized laser radiation at 308 nm have been carried out using a 1.5 cm ADA crystal which produced a 77 degree rotation. As only a 45 degree rotation is required for the optical isolator, ADA will likely be used in a prototype optical isolator for demonstration of the unstable resonator with an output ring.

Anti-Stokes Raman Scattering Introduction

Experiments have been conducted on stimulated anti-stokes Raman scattering in inverted atomic selenium to generate laser radiation at 145.7 nm. The inversion is created by photodissociation of OCSe with 193 nm laser radiation. The anti-Stokes transition is then pumped with 205 nm radiation. We have studied the conversion efficiency and tunability as a function of OCSe pressure, pump intensity, photodissociation intensity, and relative timing of the pump and photodissiciation lasers. We have also studied the effects of adding various buffer gasses, such as CO and argon, to the OCSe. Investigations of competing processes have also been conducted, and several cascade processes leading to direct laser action which strongly competes with the anti-Stokes Raman process on exact resonance have been identified.

Experimental Setup

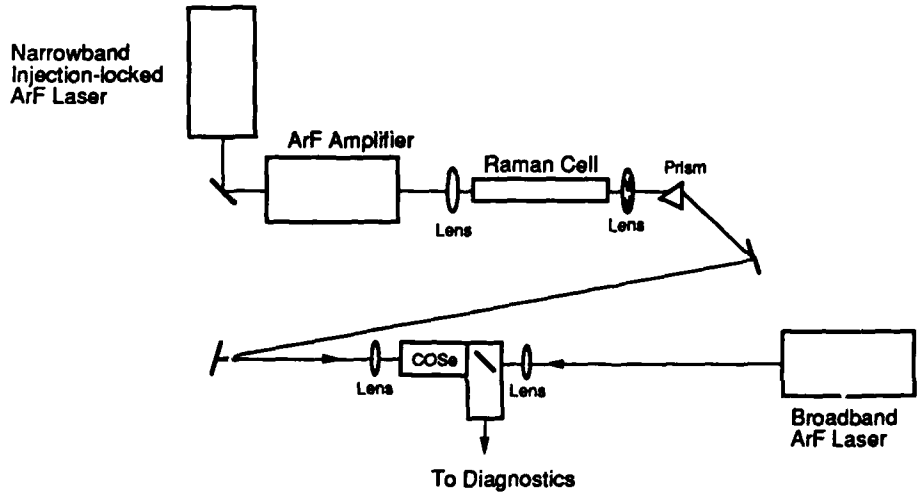

146 nm Signal Dependence on pump energy at 193nm

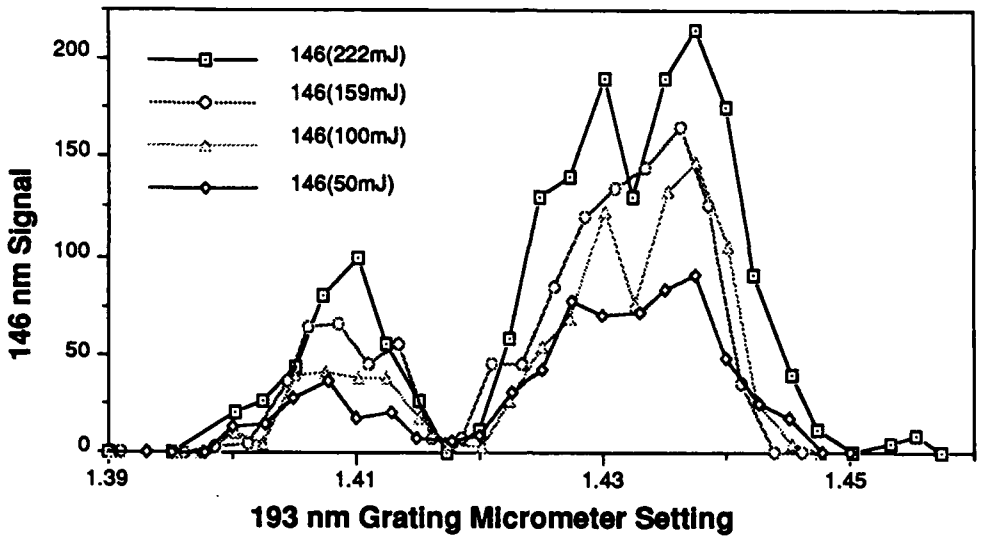

146 nm Signal vs OCSe Pressure

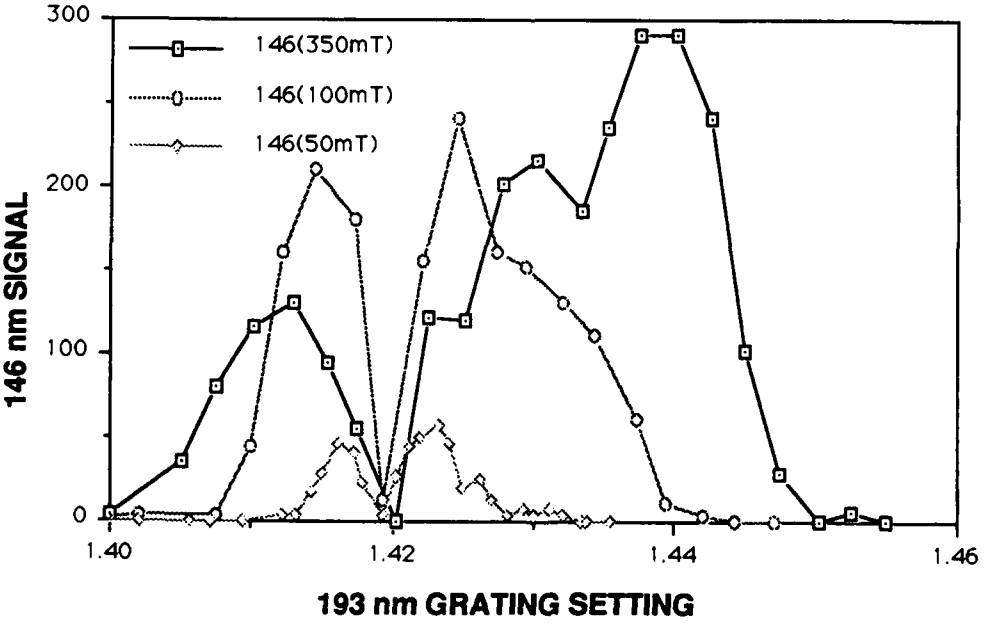

146 nm Signal Dependence on the OCSe : CO ratio

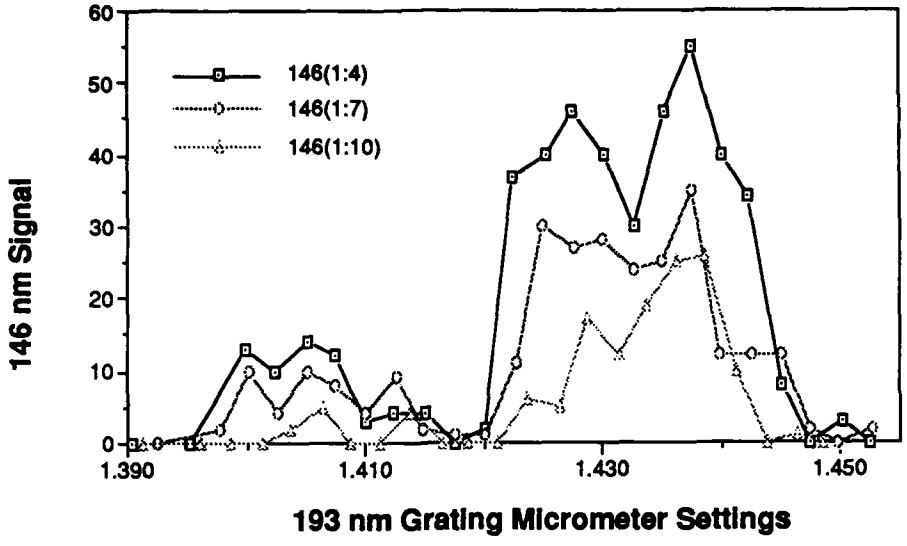

146 nm and IR Signals vs Grating setting for 350 mT OCSe

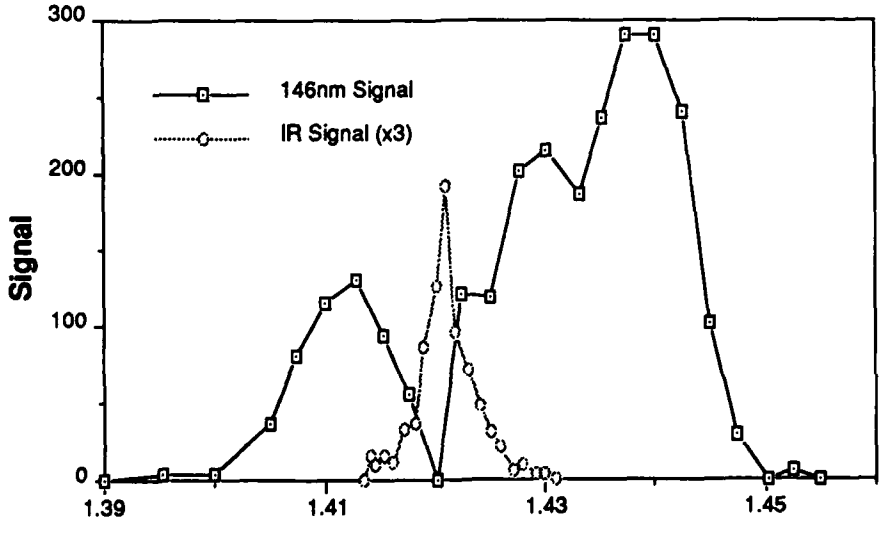

146 nm Signal Dependence on Ar Pressure

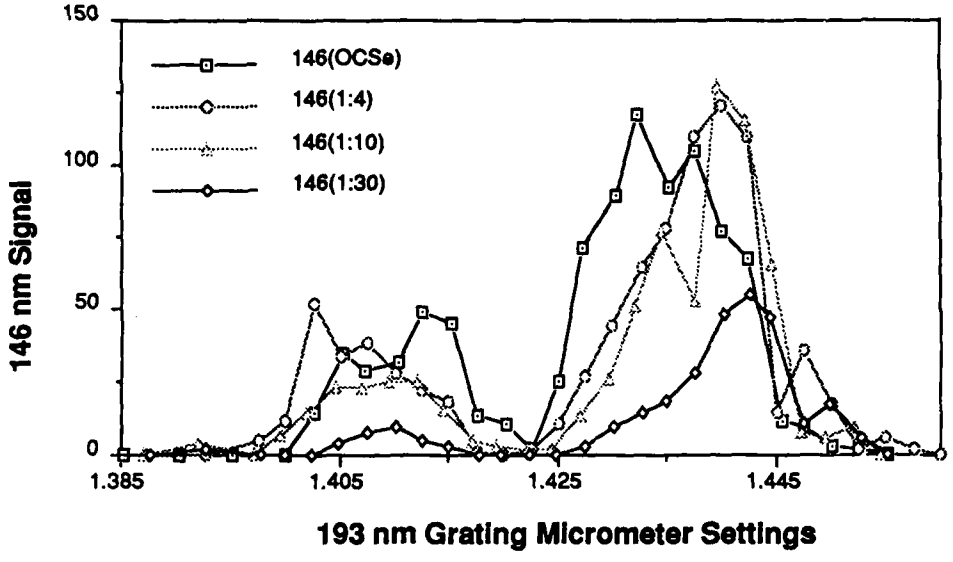

146 nm Signal Dependence on Timing

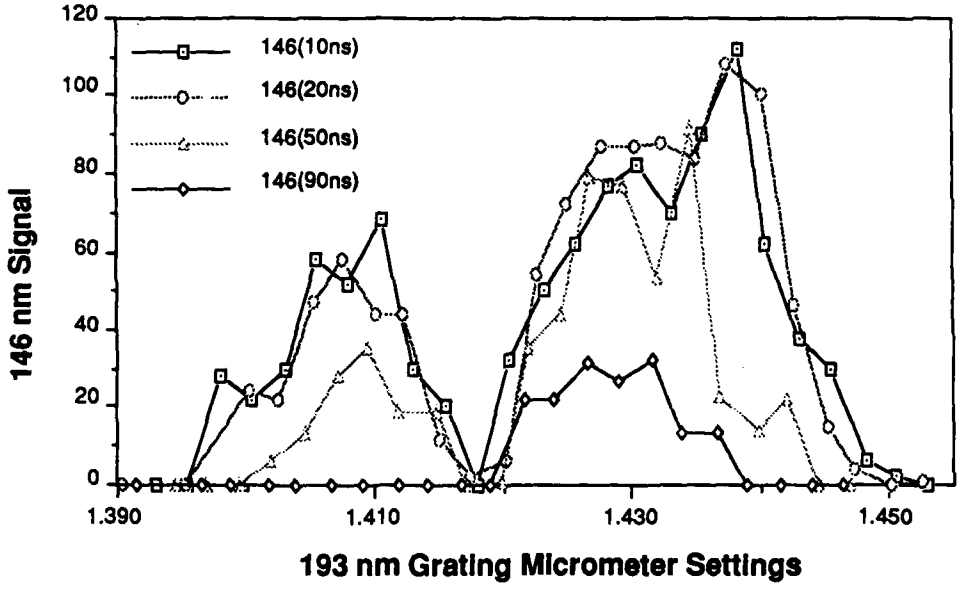

Selenium Laser Transitions Observed on Exact Pump Resonance

λ_{air}	Transition
6.369 μm	$4p^3(^2P^\circ)5s\ ^3P^\circ_1 \rightarrow 4p^3(^4S^\circ)6p\ ^3P_0$
6.31 μm	$4p^3(^2P^\circ)5s\ ^3P^\circ_1 \rightarrow 4p^3(^4S^\circ)6p\ ^3P_2$
6.25 μm	$4p^3(^2P^\circ)5s\ ^3P^\circ_1 \rightarrow 4p^3(^4S^\circ)6p\ ^3P_1$
3.33 μm	$4p^3(^4S^\circ)6p\ ^3P_0 \rightarrow 4p^3(^4S^\circ)6s\ ^3S^\circ_1$
1.515 μm	$4p^3(^4S^\circ)6s\ ^5S^\circ_2 \rightarrow 4p^3(^4S^\circ)5p^5P_3$
1.492 μm	$4p^3(^4S^\circ)6s\ ^5S^\circ_2 \rightarrow 4p^3(^4S^\circ)5p^5P_2$
1.482 μm	$4p^3(^4S^\circ)6s\ ^5S^\circ_2 \rightarrow 4p^3(^4S^\circ)5p^5P_1$
1.363 μm	$4p^3(^4S^\circ)6s\ ^3S^\circ_1 \rightarrow 4p^3(^4S^\circ)5p^5P_2$
1.039 μm	$4p^3(^4S^\circ)5p\ ^3P_1 \rightarrow 4p^3(^4S^\circ)5s^3S^\circ_1$
1.033 μm	$4p^3(^4S^\circ)5p\ ^3P_2 \rightarrow 4p^3(^4S^\circ)5s^3S^\circ_1$
1.031 μm	$4p^3(^4S^\circ)5p\ ^3P_0 \rightarrow 4p^3(^4S^\circ)5s^3S^\circ_1$
0.952 μm	$4p^3(^2P^\circ)5s\ ^3P^\circ_1 \rightarrow 4p^3(^4S^\circ)5p\ ^3P_0$
0.800 μm	$4p^3(^4S^\circ)5p\ ^3P_2 \rightarrow 4p^3(^4S^\circ)5s\ ^5S^\circ_2$
0.5374 μm	$4p^3(^4S^\circ)6p\ ^3P_1 \rightarrow 4p^3(^4S^\circ)5s\ ^3S^\circ_1$
0.5370 μm	$4p^3(^4S^\circ)6p\ ^3P_2 \rightarrow 4p^3(^4S^\circ)5s\ ^3S^\circ_1$
0.5365 μm	$4p^3(^4S^\circ)6p\ ^3P_0 \rightarrow 4p^3(^4S^\circ)5s\ ^3S^\circ_1$

800 nm Signal vs. 193 nm Grating Setting

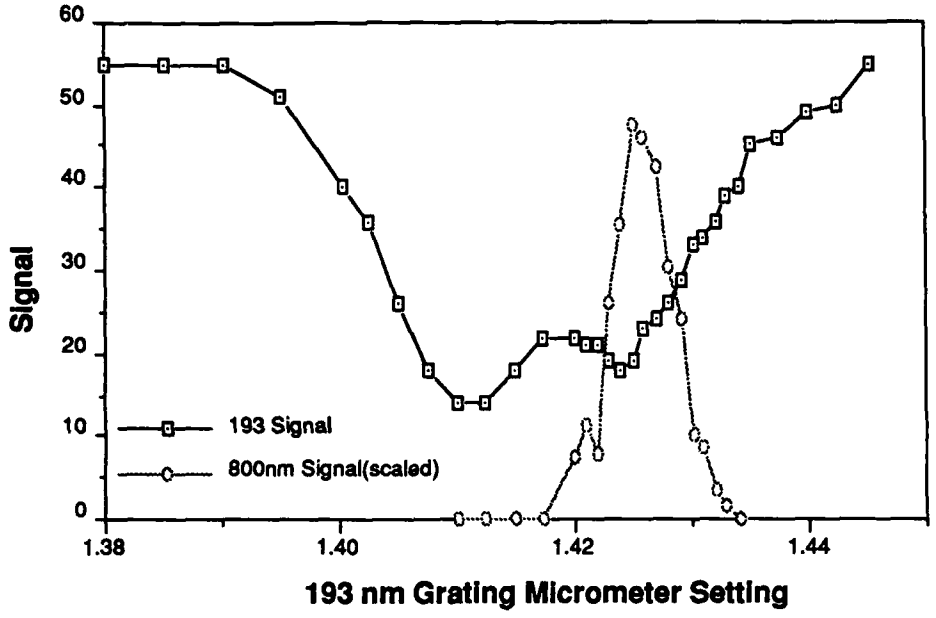

Anti-Stokes Raman Scattering Summary

Stimulated anti-Stokes Raman scattering has been observed in inverted atomic Selenium. Peak conversion efficiencies from the 205 nm pump to146 nm on the order of a few percent have been observed. The maximum tuning range obtained with 350 mTorr OCSe is approximately 20 cm-1. Studies of relative timing of the pump laser relative to the photodissociation laser have shown peak conversion efficiency for delays of 10 to 20 ns. Delays of greater than about 50 ns indicate low conversion, presumably due to strong quenching of the inverted selenium atoms by interaction with OCSe. Studies of the 146 nm generation with respect to pump and photodissociation laser intensities indicate strong saturation due of the available inverted selenium atoms. Experiments to date have shown no advantage to adding either CO or Ar as buffer gasses to the OCSe. CO appears to strongly absorb the generated radiation, while the presence of Ar appears to increase the central, resonant dip in the tuning curve, possibly due to collisional broadening of the atomic resonance.